CDDpress

Check for updates

ARTICLE

Itaconate protects ferroptotic neurons by alkylating GPx4 post stroke

Chao Wei[1,10], Zhongnan Xiao[2,10], Yanling Zhang[3,4,10], Zhaoli Luo[2,10], Dongyang Liu[5], Liye Hu[2], Danmin Shen[2], Meng Liu[1], Lei Shi[2], Xiaotong Wang[1], Ting Lan[2], Qingqing Dai[6], Jing Liu[1], Wen Chen[1], Yurui Zhang[1], Qingyu Sun[1], Weihua Wu[2], Peipei Wang[1], Chenguang Zhang [2], Junchi Hu[7], Chu Wang [3,5✉], Fei Yang [1,8✉] and Qian Li [2,9✉]

Neuronal ferroptosis plays a key role in neurologic deficits post intracerebral hemorrhage (ICH). However, the endogenous regulation of rescuing ferroptotic neurons is largely unexplored. Here, we analyzed the integrated alteration of metabolomic landscape after ICH using LC-MS and MALDI-TOF/TOF MS, and demonstrated that aconitate decarboxylase 1 (Irg1) and its product itaconate, a derivative of the tricarboxylic acid cycle, were protectively upregulated. Deficiency of Irg1 or depletion of neuronal Irg1 in striatal neurons was shown to exaggerate neuronal loss and behavioral dysfunction in an ICH mouse model using transgenic mice. Administration of 4-Octyl itaconate (4-OI), a cell-permeable itaconate derivative, and neuronal Irg1 overexpression protected neurons in vivo. In addition, itaconate inhibited ferroptosis in cortical neurons derived from mouse and human induced pluripotent stem cells in vitro. Mechanistically, we demonstrated that itaconate alkylated glutathione peroxidase 4 (GPx4) on its cysteine 66 and the modification allosterically enhanced GPx4's enzymatic activity by using a bioorthogonal probe, itaconate-alkyne (ITalk), and a GPx4 activity assay using phosphatidylcholine hydroperoxide. Altogether, our research suggested that Irg1/itaconate-GPx4 axis may be a future therapeutic strategy for protecting neurons from ferroptosis post ICH.

INTRODUCTION

Intracerebral hemorrhage (ICH) is a severe subtype of stroke with high morbidity and mortality but no effective treatment [1–3]. Current therapeutic interventions focus on decreasing secondary damage, including reducing intracranial pressure, decreasing inflammation response, promoting neuronal protection, and inhibiting neuronal cell death. There are various neuronal cell death pathways, including apoptosis, necrosis [4, 5], autophagy [5, 6], and ferroptosis [7, 8], resulting in neurologic deficits after ICH [4, 8]. Neuronal ferroptosis is one of the important modes of cell death following ICH, depending on intracellular iron overload [7, 8], and triggered by uncontrolled lipid peroxidation [4, 8]. Glutathione peroxidase 4 (GPx4) is a core regulator in ferroptosis in response to ICH. Recent studies have demonstrated that overactivated lipoxygenase [8, 9] and impaired GPx4 activity [10–12] lead to lipid reactive oxygen species (ROS) accumulation and neuronal ferroptosis in ICH. In contrast, sufficient intracellular glutathione (GSH) and selenium administration maintain GPx4 activity and inhibit ferroptosis [10].

Cellular metabolism is disturbed in ferroptotic cells. In the mitochondria, adenosine triphosphate (ATP) production relies on the tricarboxylic acid (TCA) cycle, electron transport chain (ETC), and oxidative phosphorylation. Electron transport is a series of redox reactions, and ROS is the side product of oxidative phosphorylation. Previous research reported that inhibition of the mitochondrial ETC complexes selectively inhibits ferroptosis caused by cysteine starvation [13, 14]. Mitochondria play important roles in promoting cysteine deprivation-induced ferroptosis in cancer cells [13]. However, whether metabolites in the TCA cycle are involved in neuronal ferroptosis remains unknown. Itaconate is an intermediate metabolite in the TCA cycle that is produced from cis-aconitate by the enzyme immuneresponsive gene 1 (Irg1, encoded by Acod1) in mitochondria [15]. It has been reported to reprogram glycometabolism by alkylating various enzymes (ALDOA [16, 17], GAPDH [18], SDH [19], and LDHA [17]) and suppress inflammation by affecting the IκBζ-ATF3 [20] or Keap1/Nrf2 axis [21] in macrophages.

[1]Department of Neurobiology, School of Basic Medical Sciences, Capital Medical University, Beijing 100069, China. [2]Department of Biochemistry and Molecular Biology, School of Basic Medical Sciences, Capital Medical University, Beijing 100069, China. [3]Peking-Tsinghua Center for Life Sciences, Academy for Advanced Interdisciplinary Studies, Peking University, Beijing 100871, China. [4]State Key Laboratory of Bioactive Substance and Function of Natural Medicines, Institute of Materia Medica, Chinese Academy of Medical Sciences and Peking Union Medical College, Beijing 100050, China. [5]Synthetic and Functional Biomolecules Center, Beijing National Laboratory for Molecular Sciences, Key Laboratory of Bioorganic Chemistry and Molecular Engineering of Ministry of Education, College of Chemistry and Molecular Engineering, Peking University, Beijing 100871, China. [6]Department of Geriatrics, Beijing Tsinghua Changgung Hospital, School of Clinical Medicine, Tsinghua University, Beijing 102218, China. [7]Basic Medicine Research and Innovation Center for Novel Target and Therapeutic Intervention, Ministry of Education, Institute of Life Sciences, Chongqing Medical University, Chongqing 400010, China. [8]Laboratory for Clinical Medicine, Beijing Key Laboratory of Neural Regeneration and Repair, Capital Medical University, Beijing 100069, China. [9]Beijing Key Laboratory of Cancer Invasion and Metastasis Research, Beijing Key Laboratory of Neural Regeneration and Repair, Laboratory for Clinical Medicine, Capital Medical University, Beijing 100069, China. [10]These authors contributed equally: Chao Wei, Zhongnan Xiao, Yanling Zhang, Zhaoli Luo. ✉email: chuwang@pku.edu.cn; feiyang@ccmu.edu.cn; qianli@ccmu.edu.cn

Recent studies have shown that Irg1/itaconate reprograms neuronal metabolism to protect neurons infected with Zika virus [22] and ROS-injured neurons after cerebral ischemia/reperfusion [23–25]. Itaconate inhibits ferroptosis in macrophages in a Nrf2-dependent manner [26] and mediates ferroptosis resistance in tumor-infiltrating neutrophils through the Nrf2 pathway [27]. However, little is known about whether Irg1/itaconate participates in neuronal ferroptosis and its underlying mechanisms post ICH. Furthermore, research on how to limit ferroptotic stimuli to control ICH's secondary damages, aside from canonical pathways, is lacking. The goal of this study was to investigate the effect of itaconate on neuronal ferroptosis and elucidate its underlying mechanisms, thereby advancing future clinical translational studies.

RESULTS

Irg1/itaconate level is elevated after ICH

To examine the alterations in tricarboxylic acid (TCA) metabolites in the hyperacute/acute phases following intracerebral hemorrhage (ICH), we conducted metabolomic analysis utilizing liquid chromatography coupled with mass spectrometry (LC-MS) using ICH and sham-operated ipsilateral mouse brains. Itaconate (along with pyruvate, aconitate, and fumarate) was significantly increased in response to ICH (Fig. 1A, S1A–D, and Tables S1, 2) on day 1 (the peak time for neuronal ferroptosis [8]), and only itaconate and lactate were also elevated at 6 h post-ICH (Fig. S2A–G). We utilized matrix-assisted laser desorption ionization time of flight (MALDI-TOF)/TOF MS to image coronal sections of the mouse ipsilateral hemisphere to determine the distribution of itaconate. Consistent with the LC-MS data, a significant increase in itaconate was observed after ICH, while succinate and malate levels remained uncharged (Fig. 1B and S1E–G). The elevation of itaconate was not restricted to the hematoma core and perihematomal region where reactivated microglia/infiltrated monocyte/macrophages (MMΦ) are located; itaconate was also markedly increased in the ipsilateral cortex and corpus callosum (Fig. 1C).

To determine whether the increased itaconate was caused by the upregulated expression of Irg1, we detected Irg1 in sham and ICH mouse brains at both the transcriptional and translational levels. The mRNA and protein levels of Irg1 were markedly increased on day 1 and 3 in the ipsilateral hemorrhagic brains (Fig. 1D, E). To further confirm Irg1's role as the key enzyme converting cis-aconitate to itaconate, we generated $Irg1^{-/-}$ mice and observed the expected depletion of Irg1 and itaconate in them (Fig. 1F, G).

Irg1/itaconate protects against neuronal death and improves acute outcomes after ICH

To examine whether Irg1/itaconate is beneficial or detrimental to ICH, we conducted behavioral tests pre- and post-ICH using $Irg1^{-/-}$ mice and $Irg1^{+/+}$ littermates. $Irg1^{-/-}$ mice had significantly lower forelimb placing score, higher hindlimb placing score, decreased latency in wire hanging test, and greater neurobehavioral deficits up to 24 h post-ICH (Fig. 2A). Since neuronal death contributes greatly to neurologic deficits, we examined neuronal survival in the perihematomal region and lesion volume after ICH. Depletion of Irg1 increased the profile of Fluoro-Jade C (FJC)$^+$ degenerating neurons (Fig. 2B), reduced the profile of cresyl violet (CV)$^+$ surviving neurons (Fig. 2C), and increased lesion volume (Fig. 2D). To investigate whether the neurologic deficits caused by Irg1-depletion could be rescued by supplementing itaconate, we administered 4-Octyl itaconate (4-OI) [21] to $Irg1^{-/-}$ mice and assessed neuronal loss and neurobehaviors. As expected, intraperitoneal (i.p.) (Fig. 2E and S3A) or intracerebroventricular (i.c.v.) (Fig. S3B–F) administration of 4-OI markedly reduced neural death and improved the acute outcomes in ICH mice. These results suggest that Irg1/itaconate exhibits endogenous beneficial effects after ICH.

To investigate whether exogenous increasing Irg1/itaconate levels protect against hemorrhagic damage, we administered 4-OI or vehicle to C57BL/6 (WT) mice via intraperitoneal injection at the onset of ICH. 4-OI delivery (100 mg/kg) significantly improved acute outcomes after ICH in a collagenase injection (Fig. 2F) and an autologous blood injection mouse model (Fig. S4A) in male mice. However, administrating effective dosage (100 mg/kg) of 4-OI to female mice (Fig. S4B), or lower dosages (10 or 50 mg/kg) of 4-OI to male mice (Fig. S5A) had no effects on behavior corrections. Consistent with the neurobehavioral improvement, WT male mice injected with 4-OI (100 mg/kg) displayed a decreased profile of FJC$^+$ degenerating neurons (Fig. 2G), increased profile of CV$^+$ surviving neurons (Fig. 2H), and decreased lesion volume (Fig. 2I) on day 1 and day 3 post-ICH, but the difference between 4-OI and vehicle group were not significant on day 7 post-ICH (Fig. S6A–E). Moreover, repeated administration of 4-OI (100 mg/kg, another dose given at 18 h after ICH onset) did not further improve neurobehavior nor did it increase neuronal survival (Fig. S5B–H). Importantly, delayed administration of 4-OI up to 4 h post-collagenase injection still effectively improved the neurologic deficits and rescued neuronal death (Fig. S6F–M). These data indicate that Irg1/itaconate protects hemorrhagic mouse brains, likely by rescuing striatal neurons at the acute phase of ICH.

Exogenous expression of Irg1 in striatal neurons relieves acute functional impairment after ICH

We assessed the distribution of Irg1 expression with fluorescence in situ hybridization. Irg1 was mainly expressed in neurons and Iba-1$^+$ MMΦ, and neuronal Irg1 mRNA level was significantly elevated at day 1 post-ICH (Fig. 3A–D). To investigate the role of Irg1 in MMΦ, We crossed Cx3cr1-creERT and Irg1$^{fl/fl}$ mice to deplete Irg1 specifically in MMΦ (referred to as Irg1$^{\Delta MM\Phi}$, Fig. 3E and S7A). Compared with control mice, depletion of Irg1 in MMΦ didn't decrease the total itaconate content nor aggravate the acute behavior deficits in ICH mice at day 1 post-ICH (Fig. 3F, G), but aggravated neuronal loss and behavior dysfunction at day 5 (Figs. S7B, C). Since itaconate mediates the anti-inflammation of macrophages in infective diseases, and inflammation leads to neuronal death post-ICH, we pharmacologically depleted MMΦ with the PLX5622 chow (Fig. 3H–J). In MMΦ-depleted mice, administration of 4-OI still effectively rescued neurobehavior deficits and neuronal death compared with the control group at day 1 post-ICH (Fig. 3K–O). These data strongly suggest that Irg1/itaconate protects against neuronal death and related neurologic functional improvement may not be directly related to MMΦ in the acute phase of ICH.

To further investigate the importance of neuronal Irg1 in vivo, we stereotactically injected pAAV-SYN-EGFP-P2A-Irg1-3FLAG viruses (referred to as Irg1$^{OE \ neuron}$) or control adeno-associated viruses (AAV) (referred to as Vector) into the left striatum of the WT mice (Fig. 4A). Irg1 overexpression was confirmed using real-time RT-PCR, Western blotting, and immunofluorescent staining (Fig. S7D–H). Next, we induced hemorrhage in mice that pre-overexpressed either neuronal Irg1 or Vector. Irg1$^{OE \ neuron}$ markedly decreased the number of degenerating neurons (Fig. 4B), increased surviving neurons (Fig. 4C), decreased lesion volume (Fig. 4D), and relieved functional impairment after ICH (Fig. 4E).

We next depleted Irg1 in striatal neurons (referred to as Irg1$^{\Delta neuron}$) by injecting AAVs containing a Cre recombinase with a syn promotor into the left striatum of Irg1$^{fl/fl}$ mice (Fig. 4F). Vector AAVs were injected and served as the control (referred to as Irg1$^{fl/fl}$). The selective depletion of neuronal Irg1 increased neuronal death (Fig. 4G, H) and lesion volume (Fig. 4I) as well as aggravated neurologic deficits and motor dysfunction (Fig. 4J) after ICH. These results indicate that striatal neuronal Irg1/itaconate prevents neuronal injuries and relieves functional impairment after ICH.
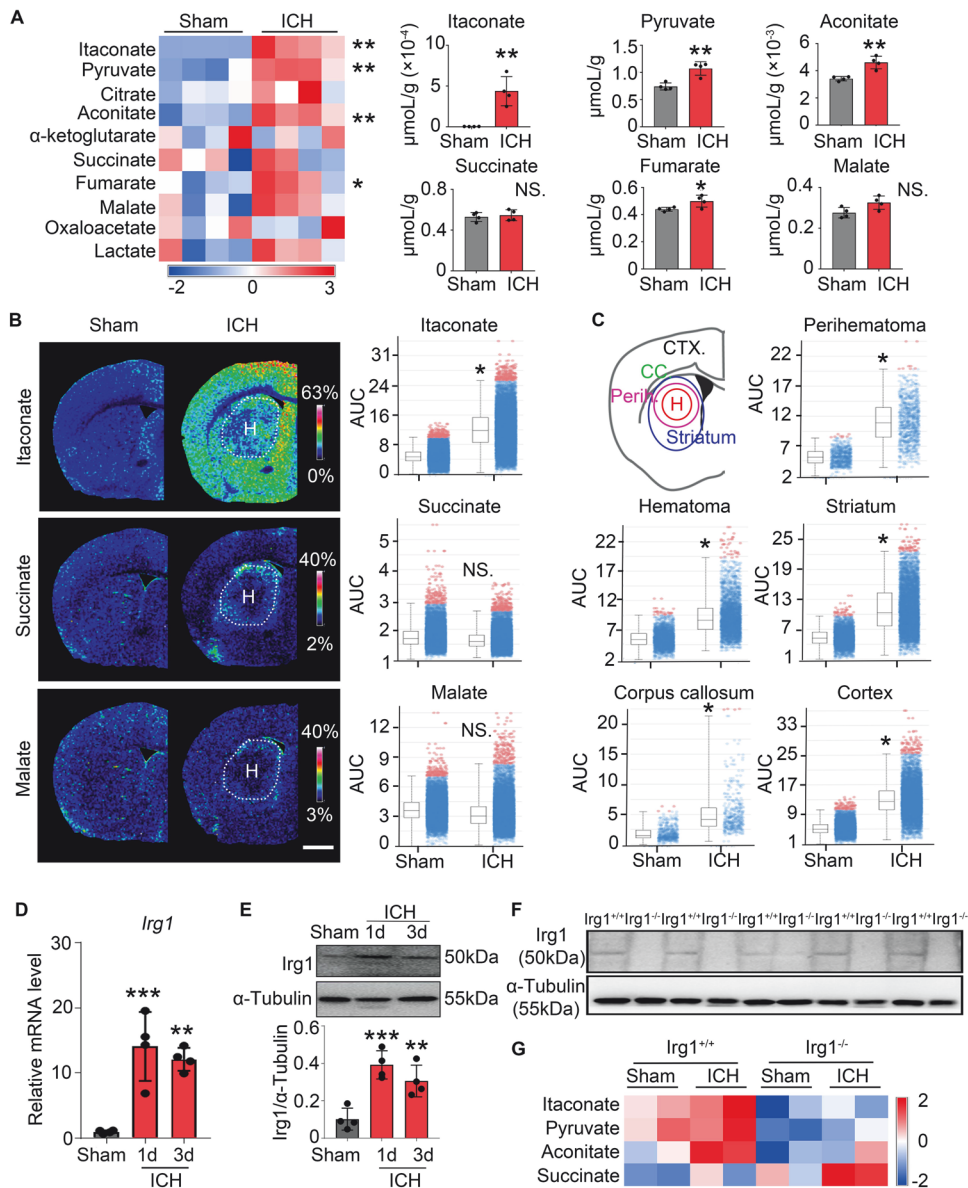
Fig. 1 Irg1/itaconate level is elevated in ICH mouse brains. A The metabolites of TCA in ipsilateral hemispheres from sham and 1-day post-ICH mice were analyzed by using LC/MS analysis. **B** The distribution and AUC values of itaconate, succinate, and malate in ipsilateral hemispheres were analyzed in sham and 1-day post-ICH mice using MALDI-TOF MS. **C** The distribution of itaconate in various brain regions of sham and ICH mice. **D** mRNA was extracted from ipsilateral striata of sham and ICH mice, and real-time RT-PCR was performed. **E** The protein level of Irg1 was analyzed from ipsilateral striata of sham and ICH mice by using Western blotting. **F** The protein level of Irg1 from *Irg1$^{-/-}$* mice and littermates (*Irg1$^{+/+}$*) was analyzed by using Western blotting. **G** The level of itaconate in ipsilateral hemisphere from *Irg1$^{-/-}$* mice and littermates (*Irg1$^{+/+}$*) at 1-day post-ICH or in sham group was analyzed by using LC/MS. **A–C** Two-tailed Student's *t*-test followed by Welch's correction. **D, E** One-way ANOVA followed by Dunn's multiple comparison post-hoc test. *$p < 0.05$, **$p < 0.01$, ***$p < 0.001$; NS. not significant. Each group contained 4 (**A, D, E**), 3 (**B, C**), 5 (**F**), or 2 (**G**) animals. Scale bar: (**B**) 1 mm.

We further conducted untargeted metabolomics using LC-MS with 4-OI- or vehicle-treated mouse brains (Figs. S8A, B). There was a significant increase of the ferroptosis pathway-related metabolites in ICH mice at 6 h, and 4-OI administration inhibited the ferroptosis pathway markedly (Figs. S8C, D), indicating that ferroptosis was involved in the protective role of itaconate.

Irg1/itaconate inhibits hemin-induced ferroptosis in mouse primary neurons and human iPSCs-derived cortical neurons in vitro

To explore the underlying neuronal protective mechanism of Irg1/itaconate in ICH, we cultured mouse neuronal cell line N2A and primary cortical neurons. Hemin is primarily employed for in vitro

modeling of ICH pathology. Hemin, as similar as canonical ferroptosis inducers, such as Erastin (a system χ_c^- cystine/glutamate antiporter blocker) and Ras-selective lethal small molecule 3 (RSL3, a GPx4 inhibitor), induced cell death in N2A cells (Fig. S9A–C) and in primary neurons (Fig. S9D–F) dose-dependently. Ferrostatin-1 (Fer-1), a specific inhibitor of ferroptosis, blocked cell death induced by hemin, Erastin, and RSL3 (Fig. S9A–F). These data suggest that a hemin-induced neuronal ferroptosis in vitro model was established.

The expression level of Irg1 was elevated in response to hemin in primary neurons time-dependently (Fig. 5A, B). Knocking down *Irg1* using siRNA (Fig. 5C) promoted hemin-induced cell death in primary neurons (Fig. 5D) and in N2A cells (Fig. S9G). In addition,
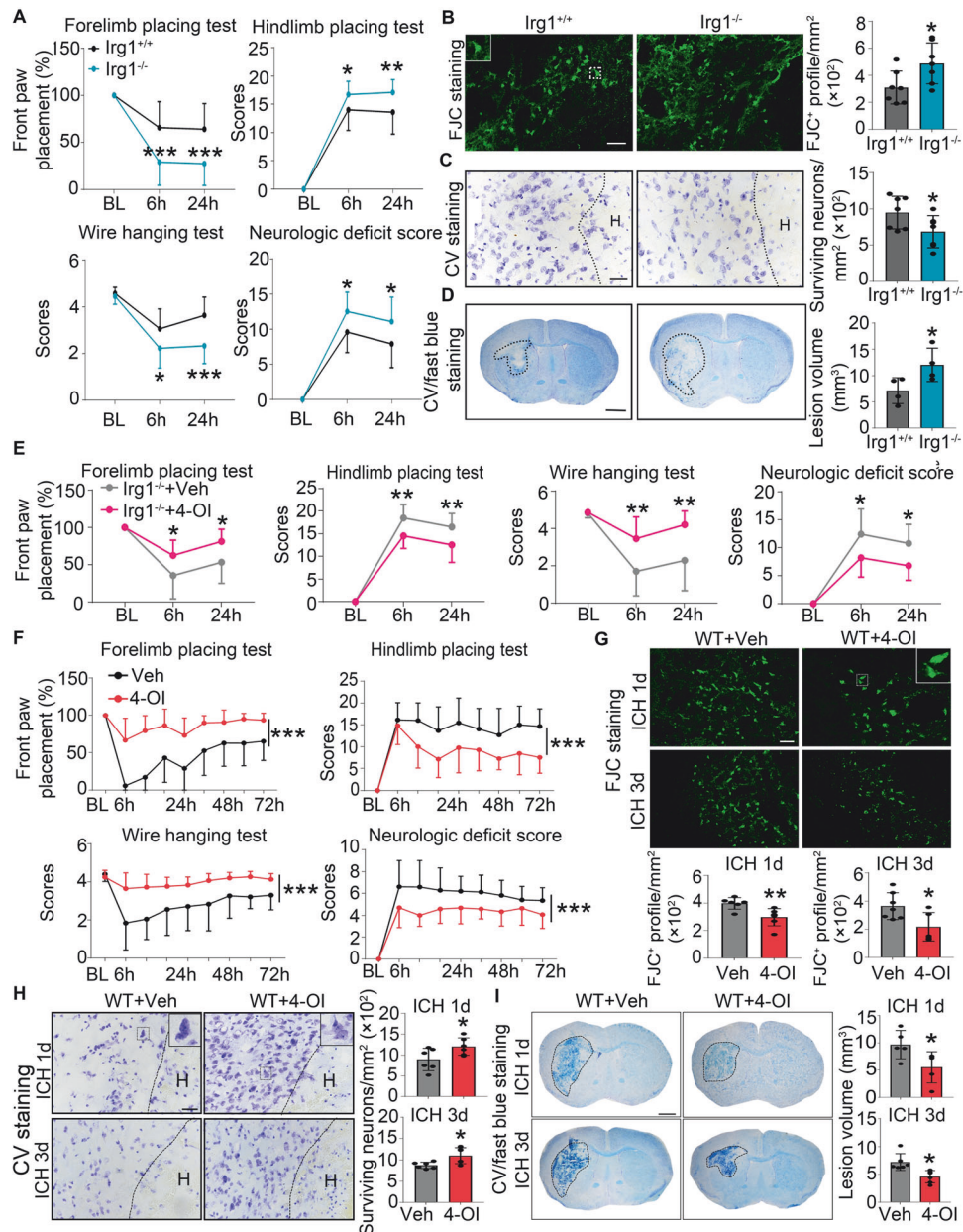
Fig. 2 Irg1/itaconate protects against neuronal death and improves acute outcomes after ICH. A Acute outcomes were examined at 6 h and 24 h after ICH between $Irg1^{-/-}$ mice and littermates ($Irg1^{+/+}$). Brain slices were obtained at day 1 after ICH and stained with (**B**) FJC, (**C**) CV, and (**D**) CV/fast blue. **E** $Irg1^{-/-}$ mice underwent collagenase injection followed by intraperitoneal injection of 4-OI or vehicle immediately after ICH onset. Acute outcomes were tested after ICH. **F–I** WT mice underwent collagenase injection, followed by intraperitoneal injection of 4-OI or vehicle immediately after ICH onset. **F** Acute outcomes were tested at different time points after ICH. Brain slices obtained at day 1 and day 3 were stained with (**G**) FJC, (**H**) CV, and (**I**) CV/fast blue. Dashed lines indicate hematoma (**C**, **H**) or lesion (**D**, **I**); H hematoma. Results are presented as line graphs or scatter plots (mean ± SD). **B**, **C**, **D**, **G**, **H**, **I** Two-tailed Student's t-test followed by Welch's correction. **A**, **E**, **F** Two-way ANOVA followed by Sidak's multiple comparisons test. *$p < 0.05$, **$p < 0.01$, ***$p < 0.001$. Each group contained 12 (**A**), 4–6 (**B**, **C**, **D**), 8–9 (**E**), 10–18 (**F**) or 5–6 (**G**, **H**, **I**) animals. Scale bars: (**B**, **C**, **G**, **H**) 50 μm; (**D**, **I**) 1 mm.

primary neurons extracted from $Irg1^{-/-}$ pups were more vulnerable to hemin treatment (Fig. 5E).

Next, we examined the effects of exogenous itaconate or 4-OI in these cultures. Itaconate and 4-OI decreased hemin-induced ferroptosis in primary neurons (Fig. 5F and S9H, K) and N2A cells (Figs. S9I, J). Administration of 4-OI significantly decreased hemin-induced lipid reactive oxygen species (ROS) and malondialdehyde (MDA) accumulation in primary neurons (Fig. 5G, H). Similar results were obtained in the Fer-1 group (Fig. 5G and S10A). Interestingly, Fer-1 did not enhance the protective effects of 4-OI when they were applied together, indicating that the addition of 4-OI alone

was sufficient to protect against ferroptosis (Fig. S10B). In addition, both itaconate and 4-OI blocked Erastin- and RSL3-induced ferroptosis in primary neurons (Figs. S10C, D). Of note, antioxidant supplements in the culturing media didn't affect the protective role of itaconate and 4-OI on ferroptotic neurons (Figs. S10E, F). Succinate, a TCA cycle metabolite that shares structural similarity with itaconate, didn't alter hemin-induced cell death (Figs. S10G, H).

In order to determine if this process also occurs in human cells, we differentiated cortical neurons from human pluripotent stem cells (iPSCs) (Fig. 5I, J). Hemin significantly increased the
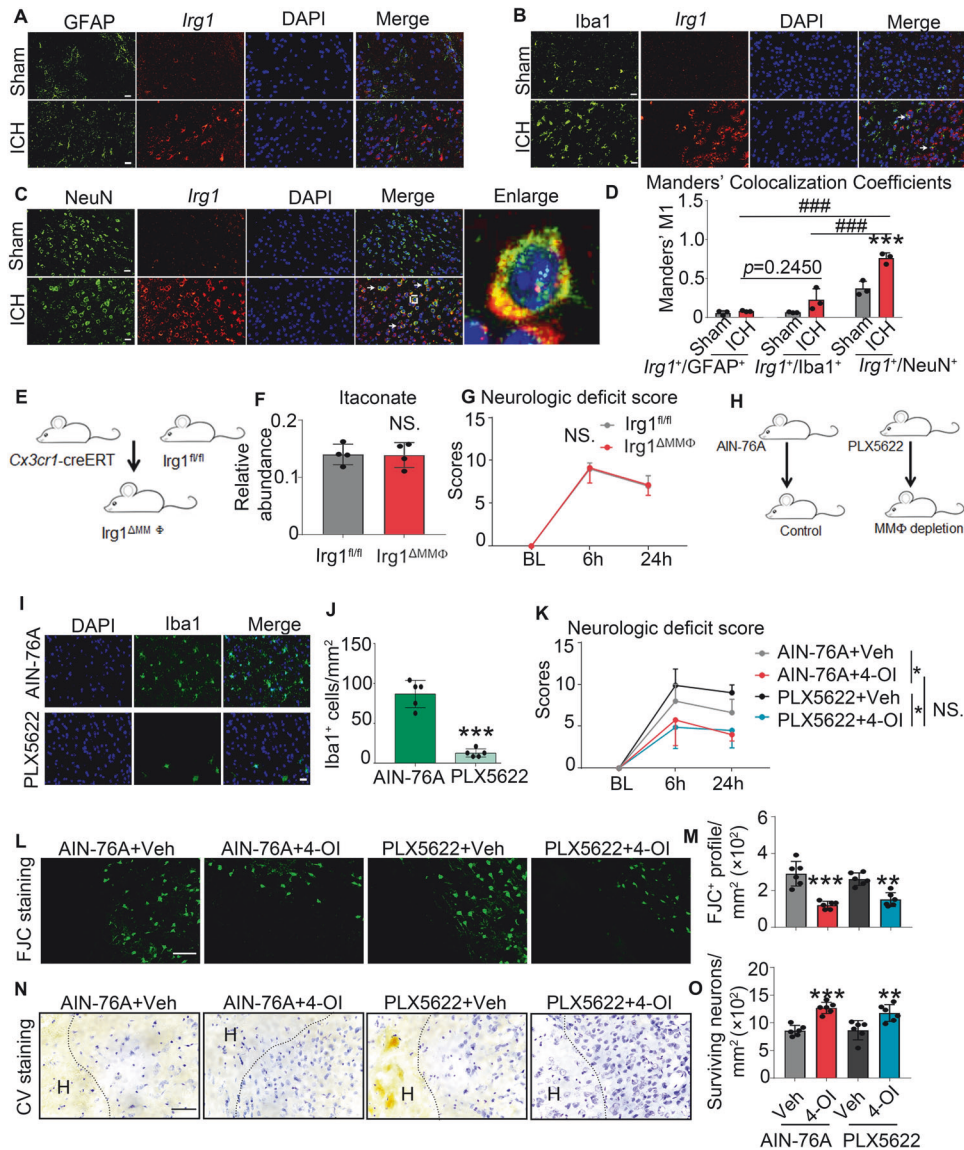
Fig. 3 Irg1/itaconate in MMΦ didn't protect acute hemorrhagic mouse brains in vivo. A–D *Irg1* expression was assessed by using fluorescence in situ hybridization (FISH). The localization of *Irg1* mRNA in astrocytes (GFAP) (**A**), microglia/macrophages (MMΦ) (Iba1) (**B**), or neurons (NeuN) (**C**) were quantified (**D**) at day 1 post-ICH. **E–G** *Cx3cr1*-creERT and Irg1$^{fl/fl}$ mice were crossed to deplete *Irg1* specifically in MMΦ (Irg1$^{\Delta MM\Phi}$). **E** Schematic procedure. **F** The concentration of itaconate in the brain of Irg1$^{fl/fl}$ and Irg1$^{\Delta MM\Phi}$ at 6 h post-ICH. **G** Acute outcomes were tested after ICH. **H–O** MMΦ were pharmacologically depleted with the PLX5622 chow. **H** Schematic procedure. **I, J** The efficiency of PLX5622 was validated with immunofluorescent staining with Iba-1. **K** Acute outcomes were tested after ICH. Brain slices obtained on day 1 after ICH were stained with (**L, M**) FJC or (**N, O**) CV. Dashed lines indicate hematoma (**N**); H hematoma. Results are presented as line graphs or scatter plots (mean ± SD). **D, G, K, M, O** Two-way ANOVA followed by Sidak's multiple comparisons test. **F, J**: Two-tailed Student's *t*-test followed by Welch's correction. *$p < 0.05$, **$p < 0.01$, ***$p < 0.001$; ###$p < 0.001$; NS. not significant. Each group contained 3 (**D**), 4 (**F**), 5–7 (**G**), 5 (**J**), or 6 (**K, M, O**) animals. Scale bars: (**A–C**) 20 μm; (**I, L, N**) 50 μm.

proportion of PI$^+$ cells in a dose-dependent manner (Fig. S10I), which could be rescued by Fer-1 (Fig. S10J). 4-OI prevented hemin-induced ferroptosis significantly (Fig. 5K and S10K). These results confirm that itaconate is an important mediator for suppressing ferroptosis in rodent and human neurons.

Irg1/itaconate's protective effect on ferroptosis is neither mediated through the Keap1/Nrf2 pathway nor mitochondrial respiration in vitro

We next set out to investigate the underlying molecular mechanisms of itaconate's protective effect on neuronal ferroptosis. Nuclear factor erythroid2-related factor 2 (Nrf2) is one of the key regulators in preventing ferroptosis during hemorrhagic pathogenesis. We extracted mRNA from hemin-treated WT

neurons and performed RNA-seq to detect the expression of Keap1/Nrf2-regulated genes. The purity of neuronal cultures was validated (Fig. S11A, B). Hemin elevated the mRNA levels of Nrf2-targeted genes, but 4-OI did not alter these gene changes when it was added to cells with hemin (Fig. S11C). We also measured the expression levels of *xCT* and *GPx4*, two vital anti-ferroptotic genes that are regulated by Nrf2. Consistent with the RNA-seq results, 4-OI did not cause *xCT* and *GPx4* changes in either mRNA (Fig. S11D, E) or protein levels (Fig. S11F, G). In addition, blocking the Nrf2 transcription activity with ML385 neither affected hemin-induced cell death nor altered the protective effect of 4-OI (Figs. S11H, I).

It has been reported that 4-OI (~125 μM) inhibits glycolysis, blocks TCA cycle, and suppresses oxidative phosphorylation in
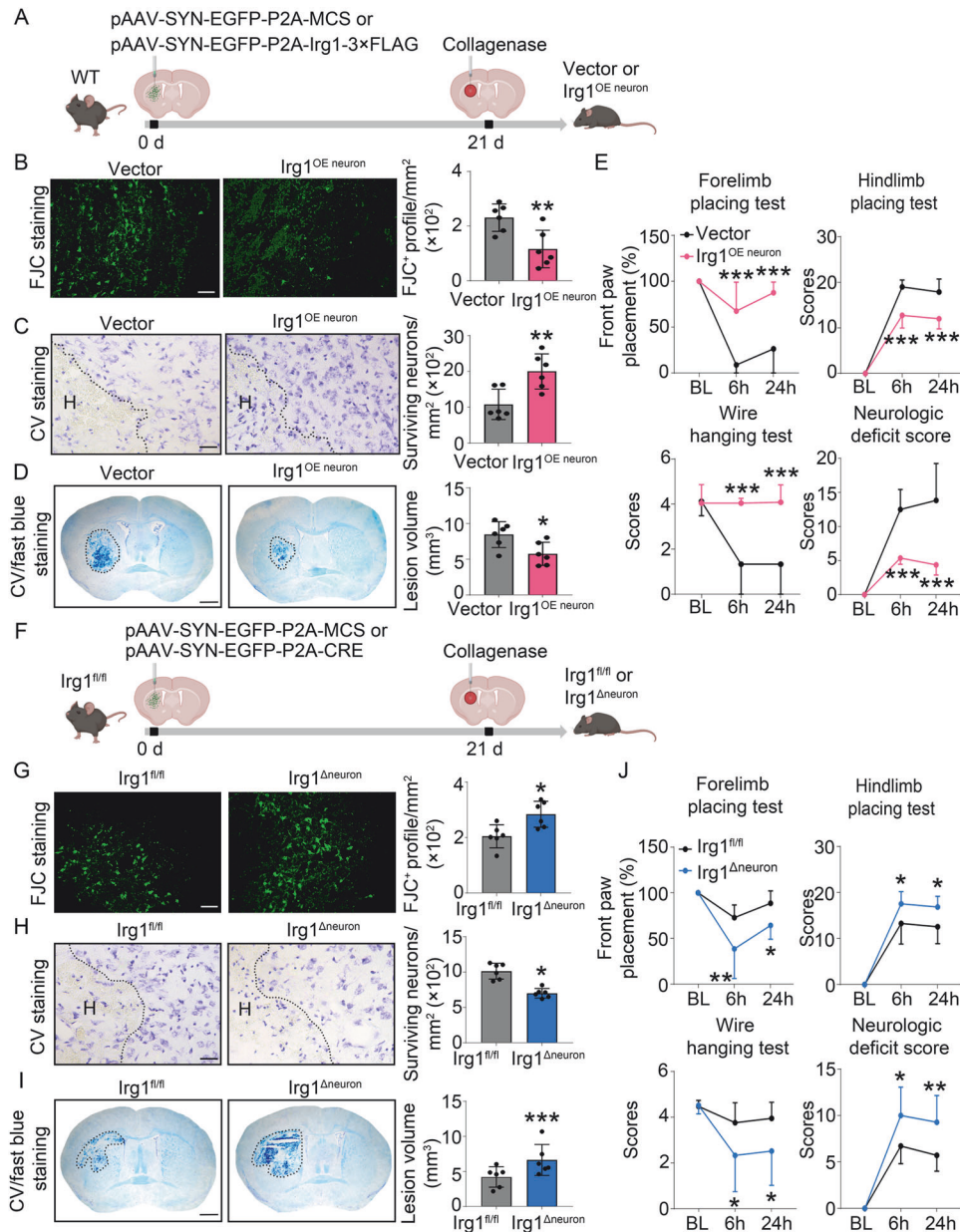
Fig. 4 Neuronal Irg1/itaconate protects hemorrhagic mouse brains in vivo. A–E pAAV-SYN-EGFP-P2A-Irg1-3FLAG (Irg1^OE neuron) and control AAV (referred to as Vector) were injected into WT mouse striata. Irg1^OE neuron or control mice underwent collagenase injection 3 weeks after virus injection. **A** Schematic procedure. Brain slices were obtained at day 1 after ICH and stained with (**B**) FJC, (**C**) CV, and (**D**) CV/fast blue. **E** Acute outcomes were tested after ICH. **F–J** *Irg1^fl/fl* mice injected with pAAV-SYN-EGFP-P2A-CRE (Irg1^Δneuron) or control AAV (referred to as *Irg1^fl/fl*) underwent collagenase injection 3 weeks later. **F** Schematic procedure. Brain slices obtained at day 1 after ICH were stained with (**G**) FJC, (**H**) CV, and (**I**) CV/fast blue. **J** Acute outcomes were tested at after ICH. Dashed lines indicate hematoma (**C, H**) or lesion (**D, I**); H hematoma. Results are presented as line graphs or scatter plots (mean ± SD). **B, C, D, G, H, I** Two-tailed Student's *t*-test followed by Welch's correction. **E, J** Two-way ANOVA followed by Sidak's multiple comparisons test. *$p < 0.05$, **$p < 0.01$, ***$p < 0.001$. Each group contained 6 (**B, C, D**), 8 (**E**), 6 (**G, H, I**) and 8 (**J**) animals. Scale bars: (**B, C, G, H**) 50 μm; (**D, I**) 1 mm.

macrophages [18]. In our experiments with neurons, hemin increased oxygen consumption rates (OCR) at 6 h and decreased it at 24 h, and the addition of 4-OI (10 μM) did not alter OCR in both time points (Fig. S12A–E and I–M). Surprisingly, hemin reduced extracellular acidification rates (ECAR) at 6 h, and 4-OI reversed the decrease (Fig. S12F–H and N–P). Since lactate failed to protect against hemin-induced neuronal death (data not shown), itaconate may rescue neuronal ferroptosis in a lactate-independent manner. Altogether, these data suggest that itaconate protects against hemin-induced neuronal ferroptosis through previously unknown mechanisms.

Itaconate increases GPx4 activity by covalently alkylating cysteine residue 66

GPx4 deficiency is the major cause of neuronal ferroptosis and can also be caused by glutathione depletion [11, 28]. GPx4 activity was markedly impaired in hemin-exposed neurons, and addition of 4-OI increased GPx4 activity significantly in both presence and absence of hemin (Fig. 6A). In addition, we performed GPx4 enzymatic activity assay in vitro using phosphatidylcholine hydroperoxide (PCOOH) consumption, a GPx4 specific substrate. Consistent with the previous results, hemin decreased GPx4 activity and 4-OI rescued hemin-reduced GPx4 activity (Fig. S13A).
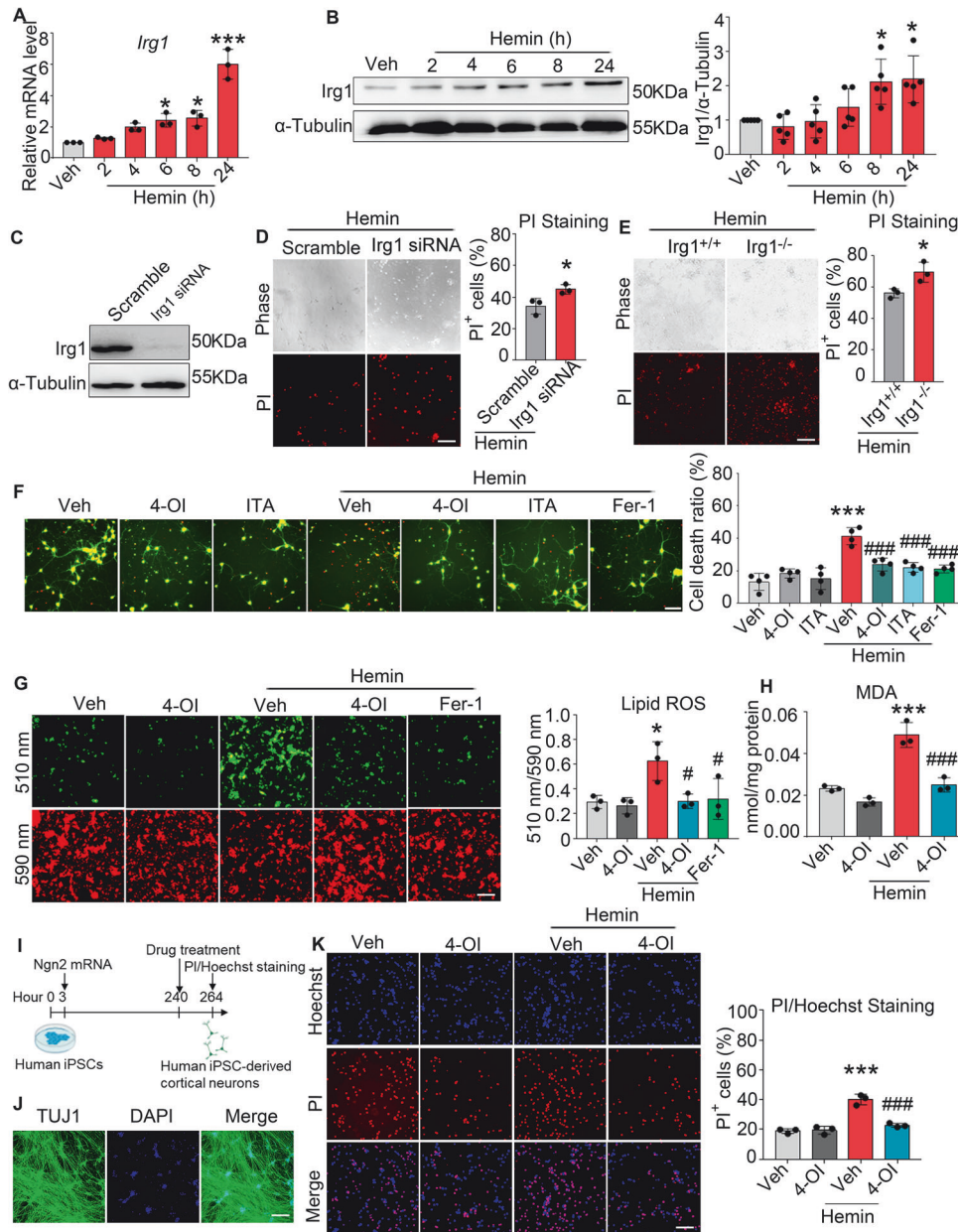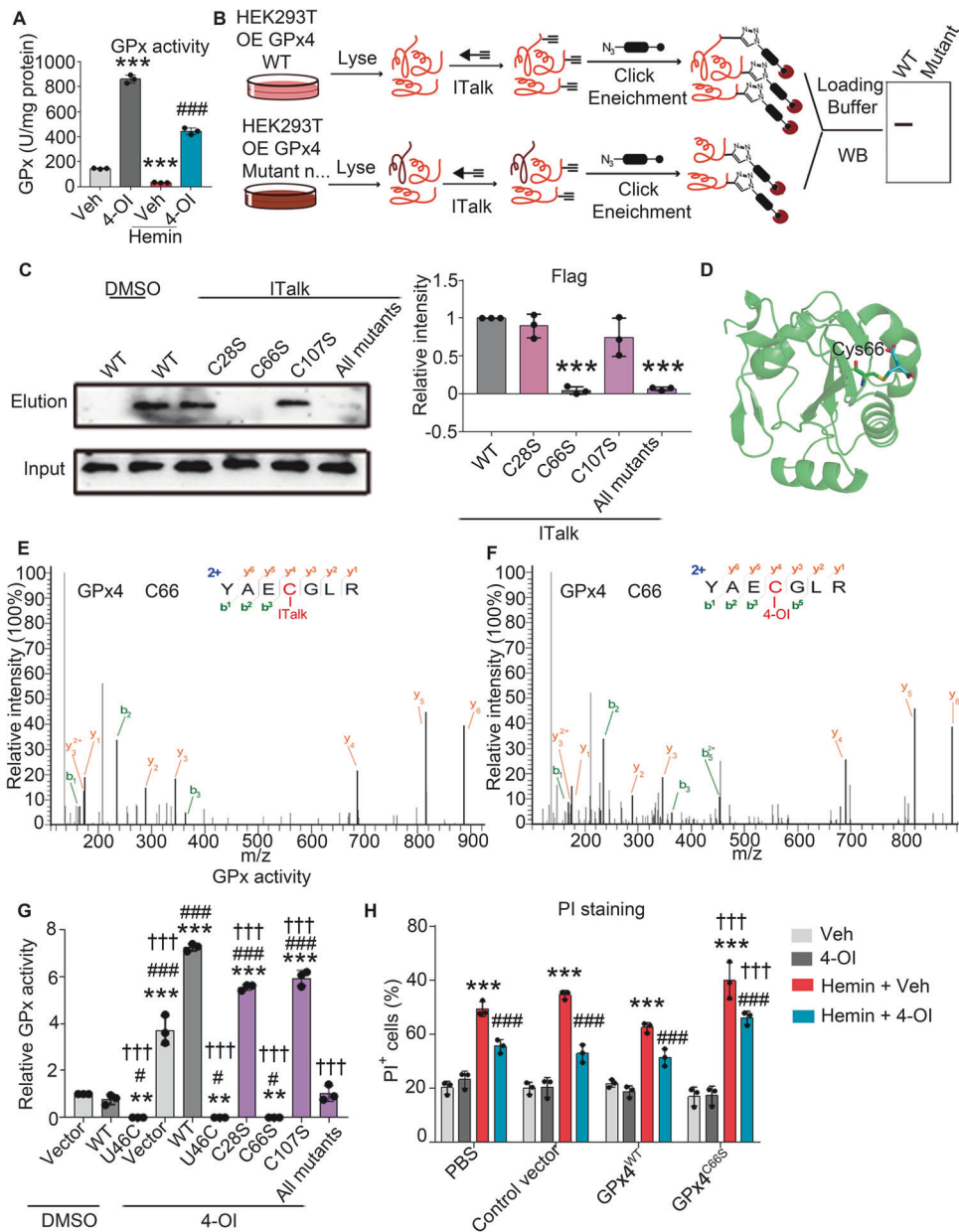
Fig. 5 Irg1/itaconate protects against hemin-induced ferroptosis in vitro. A–D WT mouse primary cortical neurons were incubated with the indicated treatment for 24 h. The levels of mRNA (**A**) and proteins (**B**) of *Irg1* were examined at different time points post application. **C, D** WT neurons were transfected with Scramble or *Irg1* siRNA for 48 h. Knockdown efficiency (**C**) and cell death rate (**D**) were assessed in the indicated group after 24 h incubation. **E** Neurons extracted from *Irg1*$^{-/-}$ pups and littermates were incubated with the indicated treatment for 24 h before performing PI staining. WT neurons were incubated with the indicated treatment for 24 h. Live/Dead assay (**F**), lipid ROS (**G**), and MDA content (**H**) were assessed. **I** Schematic procedure. **J** Human neurons were immunostained for neuronal markers TUJ1. **K** Human neurons were incubated with the indicated treatment for 24 h and PI/Hoechst staining was performed. Results are presented as scatter plots (mean ± SD). **A, B, F, G, H, K** One-way ANOVA followed Tukey's multiple comparisons test. **D, E** Two-tailed Student's *t*-test followed by Welch's correction. *$p < 0.05$, **$p < 0.01$, ***$p < 0.001$ *vs.* Vehicle/Scramble; #$p < 0.05$, ###$p < 0.001$ *vs.* Hemin + Vehicle. Each experiment was repeated 3 (**A, D, E, F, G, H, K**) or 5 (**B**) times independently. Scale bars: (**D–G, J, K**) 100 μm.

Unexpectedly, compared with hemin or ICH mice, 4-OI didn't increase glutathione content significantly in vivo (Fig. S13B–E) and in vitro (Fig. S13F).

Itaconate has electrophilic properties and alkylates cysteine residues on various proteins [18, 20, 21]. We hypothesized that itaconate alkylates GPx4 cysteine(s) and this covalent modification affects GPx4 activity. To test such a hypothesis, we first constructed single or triple cysteine-to-serine mutants near its active-site selenocysteine 46 and generated stable cell lines in HEK293T cells (GPx4^{C28S}, GPx4^{C66S}, GPx4^{C107S}, GPx4$^{C28S/C66S/C107S}$)

(Figs. S14A, B). We next used a bioorthogonal itaconate analogue probe, ITalk [29] to label and enrich WT and mutant GPx4 (Fig. 6B). Immunoblotting results showed that ITalk successfully labeled and pulled out GPx4^{WT}, GPx4^{C28S}, and GPx4^{C107S}, but not GPx4^{C66S} nor GPx4$^{C28S/C66S/C107S}$ (Fig. 6C), suggesting Cys66 is the major site covalently targeted by ITalk. In agreement with these observations, we also successfully simulated itaconate covalently binding to the sulfhydryl group on Cys66 of GPx4 (Fig. 6D). Lastly, itaconation on Cys66 of GPx4 was unambiguously successfully detected by LC/MS-MS (Fig. S14C) using a purified GPx4^{U46C}

Fig. 6 Itaconate increases GPx4 activity by covalently alkylating cysteine residue 66 on GPx4 in vitro. A WT neurons were incubated with the indicated treatment for 24 h. GPx4 enzyme activity was measured. **B** Schematic procedure to identify GPx4's itaconation with the ITalk probe. **C** HEK293T cells were infected with GPx4^{WT} (referred to as WT) and indicated mutants. After incubating with the ITalk probe or vehicle for 2 h, the probe-labeled proteins were detected by Western blotting. **D** Covalent docking results of itaconate (green cartoons) to GPx4 (cyan sticks). Cys66 of Gpx4 is shown as green sticks. A purified GPx4^{U46C} protein was incubated with ITalk (**E**) or 4-OI (**F**) for 4 h and analyzed using LC-MS/MS. **G** HEK293T cells were transfected with GPx4^{WT} and indicated mutants. Cells were treated with 4-OI or vehicle for 24 h and GPx4 activity was assessed. **H** WT neurons were infected with GPx4^{WT} and GPx4^{C66S}. Cells were treated as indicated for 24 h and PI staining was performed. **A, C, G** One-way ANOVA followed by Tukey's multiple comparisons test; **H** Two-way ANOVA followed by Tukey's multiple comparisons test. ******$p < 0.01$, *******$p < 0.001$ *vs.* Vehicle (**A**), WT (**C**), Vector+DMSO (**G**), or corresponding Vehicle (**H**); #$p < 0.05$, ##$p < 0.01$, ###$p < 0.001$ *vs.* Hemin (**A**), WT + DMSO (**G**), or corresponding Hemin (**H**); †††$p < 0.001$ *vs.* WT + 4-OI (**G**), or corresponding treatments in GPx4^{WT} (**H**). Each experiment was repeated 3 (**A, C, G, H**) times independently.

(selenocysteine to cysteine) mutant protein treated with either ITalk (Fig. 6E) or 4-OI (Fig. 6F). To demonstrate whether endogenous itaconate modified GPx4, we performed a competition experiment between itaconate and the ITalk probe. The results indeed showed that adding exogenous itaconate into the GPx4-overexpressing HEK293T lysates markedly decreased the labeling of ITalk on GPx4 (Fig. S14D). In addition, the alkylation of GPx4 was also detectable in the WT mouse brain tissue lysates

with ITalk (Fig. S14E), suggesting that GPx4 could be alkylated by itaconate in vitro and in vivo.

Consistent with the covalent modification on Cys66 of GPx4 by itaconate, we found that GPx4 activity could be enhanced by 4-OI in HEK293T cells stably transfected with GPx4^{WT} and the C66S mutants (either GPx4^{C66S} or GPx4$^{C28S/C66S/C107S}$) completely abolished the activation effect as the U46C mutant did (Fig. 6G). We also found that 4-OI treatment dose-dependently increased

Fig. 7 Irg1/Itaconate increases GPx4 activity and rescues neuronal ferroptosis in vivo. A–E WT mice were injected with GPx4^{WT} or GPx4^{C66S} viruses and underwent collagenase injection 3 weeks later. 4-OI was intraperitoneally injected immediately after ICH onset. **A, B** Brain slices obtained at day 1 after ICH were stained with FJC. Representative images (**A**) and quantifications (**B**) are shown. **C, D** Brain slices were immunostained with MDA and NeuN. Representative images (**C**) and quantifications (**D**) are shown. **E** Acute outcomes were tested after ICH. **F–M** Ipsilateral hemispheres obtained from indicted mice at 1-day post-ICH. GPx4 activity **F–I** and MDA content (**J–M**) were measured. Results are presented as line graphs or scatter plots (mean ± SD). **B, D, F–M** Two-tailed Student's *t*-test followed by Welch's correction; **E** Two-way ANOVA followed by Sidak's multiple comparisons test. *$p < 0.05$, **$p < 0.01$, ***$p < 0.001$. Each group contained 5 (**B, E**), 4 (**D**), or 5–6 (**F–M**) animals. Scale bars: (**A, C**) 50 μm.

the activity of purified GPx4 (Fig. S14F). We further infected primary neurons with lentiviruses encoding GPx4^{C66S} or GPx4^{WT}, and found that the protective effects of 4-OI were blunted in the GPx4^{C66S} group (Fig. 6H).

To determine whether Cys66 controls Irg1/itaconate-improved functional outcomes after ICH in vivo, we injected GPx4^{WT} and GPx4^{C66S} lentiviruses into the striatum of WT mice and performed an ICH model after 3 weeks. Consistent with the in vitro results, 4-OI failed to decrease the degeneration of neurons (Fig. 7A, B), neuronal MDA content (Fig. 7C, D), or to improve ICH acute outcomes (Fig. 7E) in GPx4^{C66S}-injected mice. Furthermore, we knocked down the endogenic GPx4 and then injected the GPx4^{WT} and GPx4^{C66S} viruses in ipsilateral striatal neurons in WT mice, and we obtained consistent results (Fig. S15A–D).

Finally, to assess the relevance of Irg1/itaconate on GPx4 activity and MDA content after ICH in vivo, we administered 4-OI (*i.p.*) or overexpressed *Irg1* in striatal neurons. GPx4 activity was significantly elevated (Fig. 7F, G) and MDA accumulation was reduced (Fig. 7J, K) in both approaches. On the other hand, deficiency of *Irg1* impaired GPx4 activity (Fig. 7H) and increased MDA content (Fig. 7L). Exogenous 4-OI in *Irg1*$^{-/-}$ mice reversed

GPx4 impairment and decreased MDA accumulation (Fig. 7I, M). Overall, our results demonstrate that Irg1/itaconate blocks hemin-induced ferroptosis and protects against negative hemorrhagic brain effects by alkylating Cys66 on GPx4 to enhance GPx4 activity.

DISCUSSION

Itaconate, an important tricarboxylic acid (TCA) cycle derivative, plays a wide range of roles in bacterial/virus infection [21, 30, 31], reprogramming glycolysis [18], and inhibiting inflammation [32] in macrophages. The roles of itaconate and Irg1 in the acute phases following intracerebral hemorrhage (ICH) are largely unknown. Here, we found that Irg1 expression and itaconate content were relatively low in physiological conditions in the brain tissue, but were significantly elevated in the ipsilateral hemisphere after ICH. We built on evidence of the elevation of itaconate not only in the hematoma/perihematomal regions where activated MMΦ were recruited to, but also in the ipsilateral cortex and corpus callosum. According to the results from global and conditional *Irg1*$^{-/-}$ knockout mice, lack of neuronal itaconate aggravated neurologic

deficits and neuronal loss in acute phase of ICH. Our in vivo results also demonstrated that exogenous itaconate supplementation and selective increase of neuronal itaconate were sufficient for biological protection after ICH. We demonstrated the beneficial function of endogenous and exogenous itaconate after ICH in vivo. Of note, our in vivo LC-MS data showed that hemorrhage elevated carbon source through metabolic reprogramming, and when lacking the itaconate-mediated feedback mechanism by Irg1 knockout, carbon source was also significantly decreased. These results suggested that increased itaconate might not be solely caused by Irg1 upregulation. Our data provide robust evidence that advances the understanding of the interaction between TCA metabolites and neuronal ferroptosis after ICH. Although MMΦ-originated itaconate and MMΦ did not affect neuronal death and behavior deficits in the hyperacute phase of ICH, we found that Irg1/itaconate significantly promoted phagocytosis in MMΦ through Keap1/Nrf2/CD36 signaling pathway, thereby promoting hematoma clearance and contributing to the hemorrhagic brain in the subacute phase [33].

After being released from lysed erythrocytes post ICH, hemoglobin can be taken up by microglia and metabolized into ferrous/ferric iron [34]. This process induces the production of lethal reactive oxygen species (ROS). These oxidative stresses may trigger various cell death pathways, including apoptosis, necrosis, and ferroptosis [8, 34–37]. Ferroptosis has been proven to contribute to neuronal death greatly after ICH [4, 8]. Ferroptosis inhibitors abrogated hemoglobin- and hemin-induced cell death by more than 80% [4]. Mice treated with Fer-1 after ICH exhibited marked brain protection and improved neurological function [8]. More importantly, deferoxamine mesylate (DFO), the iron chelator, has successfully completed phase I [38] and phase II [39] clinical trials, making targeting ferroptosis a promising therapeutic target in treating ICH patients. Recent studies show that 2-10 mM itaconate leads to cell death in neurons and cancer cells in vitro [23, 40, 41]. Interestingly, we discovered that the addition of a lower dosage of itaconate didn't cause neuronal death, but protected neurons against ferroptosis in vitro.

It has been reported that itaconate can enhance Nrf2 activity by alkylating Keap1 in macrophages [21], however, we observed that itaconate did not activate the Keap1/Nrf2 signaling pathway during rescue neuronal ferroptosis. Whether itaconate protects neuronal ferroptosis through activating the glial Nrf2 signaling pathway in vivo needs further study. In addition, previous studies have shown that itaconate reprograms glycolysis and mitochondrial respiration by alkylating various enzymes in macrophages [16–19]. However, our data from the Seahorse analyzer did not find that itaconate was able to alter mitochondrial oxygen consumption in neurons treated with hemin. These data suggest that cell-specific glycometabolic components and pathways may contribute to the selectivity of itaconate.

Impairment of GPx4 activity exacerbates ferroptosis in ICH [42]. Nrf2 transcription activity [43], selenium supplementation [10], and intracellular glutathione content regulate GPx4 deficiency-related ferroptosis. Here we found that Irg1/itaconate promotes GPx4 activity without increasing GPx4 expression levels or altering the content of GSH (the substrate of GPx4). GPx4 has three cysteine residues near the active site selenocysteine with free thiol sidechains. However, it has never been reported that itaconate covalently modifies GPx4. By using a chemical biology approach, we demonstrated that Cys66 is the primary site for itaconation, which results in an upregulation of GPx4 activity and drives the anti-ferroptotic response of itaconate after ICH in vitro and in vivo. Our findings are the first to show that GPx4 can be modified post-translationally by itaconate in neurons, and that it is possible itaconate acts as an allosteric activator of GPx4. Surprisingly, fumarate alkylates GPx4 at the same site and inhibits the activity of GPx4 in cancer cells [44]. We hypothesize that the modifications of itaconate and fumarate may lead to opposite changes in the structure or microenvironment of GPx4 that may affect substrate binding affinity or enzyme active site exposure. It would be interesting to explore in the future the detailed regulatory mechanisms between the itaconation on Cys66 and the activity changes in GPx4, such as Cryo-electron microscopy.

Our in vivo and in vitro results identified the neuroprotective role of neuronal Irg1/itaconate in the hyperacute and acute phase after ICH. We also found that Irg1/itaconate significantly promoted MMΦ phagocytosis and improved prognosis in the subacute stage of ICH in another study [33]. Whether supplementation of itaconate affects chronic outcomes, including impairments in motor function, learning and memory, mood or sensory, should also be explored.

In conclusion, we revealed the important role of Irg1/itaconate in protecting against neuronal ferroptosis and improving acute neurologic functions after ICH in vivo. The protective effect of itaconate in neurons via alkylating GPx4 Cys66 describes a novel model of regulation. Our findings shed light on the molecular mechanisms of ferroptosis and may help improve patient recovery after ICH or other central nervous system disorders associated with ferroptotic cell death, such as ischemic stroke and Alzheimer's disease, and an entirely new class of ferroptosis inhibitors may be designed in the future based on this data.

MATERIALS AND METHODS
All experiments were performed and reported in accordance with followed ARRIVE and RIGOR guidelines [45]. All procedures were approved by the Experimental Animal Ethics Committee of Capital Medical University. Anesthesia and euthanasia of animals were consulted with American Veterinary Medical Association (AVMA) Guidelines for the Euthanasia of Animals (2020). Animals that had a neurologic deficit score higher than 20 at 24 h after surgery were euthanized under deep anesthesia. Animals that died or were euthanized were excluded from the sample size. Three or more independent experiments were performed for all experiments. A power analysis based on our previous studies [8] and pilot data indicated that 8 mice/group would provide at least 80% power for detecting a 20% decrease in neurologic deficits at $\alpha = 0.05$ (2-sided). Animals and cell cultures for each group were randomized with the website www.randomization.com. Treatment, data collection, and data analyses were blinded by using different investigators or by masking sample labels.

Mice
Adult male and female mice (WT, C57BL/6J mice, 6–8 weeks) were obtained from Vital River. Cx3cr1-creERT, Irg1$^{-/-}$, and Irg1$^{fl/fl}$ mice (C57BL/6J background) were generated by Southern model organism (Shanghai, China). Briefly, CRISPR/Cas9 technology is adopted, and non-homologous recombination repair is used to introduce mutation, resulting in code reading frame shift and function loss of the Acod1 (Irg1) gene (Ensembl number: ENSMUST00000022722). To knock out Irg1 in the microglia/infiltrated macrophages (MMΦ), we crossed Cx3cr1-creERT and Irg1$^{fl/fl}$ mice to deplete Irg1 specifically in MMΦ with tamoxifen injections (150 mg/kg body weight; 20 mg/mL stock solution; T5648, Sigma-Aldrich, USA). Animals used in this study were bred and housed under specific-pathogen free conditions at Capital Medical University. Mice were housed in a regulated environment (22 ± 2 °C, 55 ± 5% humidity, and 12:12-h light:dark cycle with lights on at 8:00 am) and received a standard diet. Food and water were accessible adlibitum.

Cell cultures
The mouse neuroblastoma Neuro 2a (N2A) cell line was gift a from Dr. Junfa Li and HEK293T cell line was a gift from Dr. Wei Wang in Capital Medical University. N2A and HEK293T cell lines were maintained in DMEM (C11995500BT, Gibco, USA) with 10% FBS (10099141, Gibco) in a 5% CO_2 cell culture incubator, and passaged every 3 days.

The mouse pups (postnatal 0–1) were sterilized by 75% ethanol (ANNJET, China) and then sacrificed. The brain was placed in pre-cooling Hanks' solution (H1045-500, Solarbio, China) with ice bag pre-cooling to remove the meninges and blood vessels. Cortex was removed and cut into 1 mm pieces, and digested by 0.25% trypsin (KGY0012, keygen, China) for 10 min at 37 °C. Supernatant cells were filtered through a 70 μm mesh filter

(352350, Falcon, USA), and seeded on a poly-D-lysine (P0899, Sigma-Aldrich)–coated plates in Neurobasal medium (21103049, Gibco) (containing B27 supplement [17504044, Invitrogen, USA]). Cytarabine (PHR1787, Sigma-Aldrich) was added 24 h later to remove astrocytes. To perform cell stress experiments with primary neurons in the culturing media without the antioxidants, the medium was replaced with a B27 supplement (10889038, Gibco) which without 5 antioxidants (vitamin E, vitamin E acetate, superoxide dismutase, catalase, and glutathione). The corticostriatal cultures contained mostly neurons and <2% glia cells, as determined by immunofluorescence staining. Half of the media was changed every 3 days and cells were used at 7–10 days.

The human iPSC line iPS (IMR90)-1 (WiCell Research Institute) was infected by lentiviruses harboring doxycycline-inducible neurogenin 2. After doxycycline treatment for 6 days, neuronal precursors (3×10^5 cells/cm^2) were seeded on dishes pre-coated with poly-D-lysine (1 µg/mL) and laminin (1 µg/mL; Sigma-Aldrich) in neuron culture medium (Neurobasal medium with B27 supplement, brain-derived neurotrophic factor [20 ng/mL; PeproTech, USA], glial cell line-derived neurotrophic factor [20 ng/mL; PeproTech], L-ascorbic acid [0.2 mM; Sigma-Aldrich], dibutyryl cAMP [0.5 mM; Sigma-Aldrich], and γ-secretase inhibitor DAPT [10 µM; Stemgent, USA]) [46]. Half of the media was changed every 3 days, and neurons were matured for 20 days before use.

MycoSEQ Plus Mycoplasma Detection Kit (A57926, Thermo Fisher Scientific, USA) was routinely used to test mycoplasma contamination in cell cultures.

Drug administration
Unless indicated, N2A cells were exposed to 12 µM Hemin (16009-13-5, Frontier Scientific, USA), 10 µM 4-octyl itaconate (4-OI, HY-112675, MedChemExpress), 0.1–5 mM Diethyl succinate (HY-Y0836, MedChemExpress), 1–10 µM ML385 (HY-100523, MedChemExpress) for 24 h. Mouse primary cortical neurons were exposed to 50 µM Hemin, 5 µM Erastin (S7242, Selleck, USA), 5 µM RSL3 (S8155, Selleck), 500 µM itaconate (93598, Sigma-Aldrich), 10 µM 4-OI, 2 µM Ferrostatin-1 (Fer-1, S7243, Selleck) for 24 h. Human iPSCs-derived neurons were treated with 60 µM Hemin, 10 µM 4-OI for 24 h. HEK293T cells were treated with 10 µM 4-OI for 12 h.

For in vivo injections, different dosages of 4-OI (10, 50, or 100 mg/kg) or Veh [10% DMSO (D8418, Sigma-Aldrich) and 20% β-cyclodextrin (HY-17031, MedChemExpress) in sterile water] was administered intraperitoneally immediately after collagenase/autologous blood injection. In repeated administration experiment, 100 mg/kg 4-OI was administered at 0 and 18 h after ICH. 4-OI (100 µM, dissolved in 10% DMSO) prepared for intracerebroventricular injection (i.c.v.) administration was performed as previously described [47, 48]. Briefly, the 26-gauge needle of a 5 µL Hamilton syringe was inserted into the left lateral ventricle through a cranial burr hole at the following coordinates (0.5 mm anterior and 0.9 mm left lateral to the bregma, 2.5 mm deep under dura). A microinfusion pump was used for intracerebroventricular injection at a rate of 1 µL/min. Control vehicle (10% DMSO, diluted with ddH$_2$O) was injected by 5 µL/mice. The needle was left in place for an additional 10 min at the end of infusion and was removed over a 3 min period. The surgical wound was sealed with Super Glue.

Transfection
To knock down the expression of Irg1 in N2A and mouse primary neuronal cultures, scramble (sc-37007, Santa cruz, USA) or siRNA (sc-146287, Santa cruz) of Irg1 were incubated with Lipofectamine 2000 Transfection Reagent (11668027, Invitrogen) for 30 min and then incubated with cells for 6 h in a cell incubator before changing media.

To establish stable transfected HEK293T cells, lentiviruses were obtained from OBiO, Shanghai, China. pSlenti-EFIa-EGFP-P2A-Puro-CMV-MCS-3×FLAG (titer: 1.47E + 09 TU/mL), pSlenti-EFI-EGFP-P2A-Puro-CMV-GPx4-3×FLAG-WPRE (titer: 7.03E + 08 TU/mL), pSlenti-EFI-EGFP-P2A-Puro-CMV-GPx4 (C28S)-3×FLAG-WPRE (titer: 5.53E + 08 TU/mL), pSlenti-EFI-EGFP-P2A-Puro-CMV-GPx4 (C66S)-3×FLAG-WPRE (titer: 6.60E + 08 TU/mL), pSlenti-EFI-EGFP-P2A-Puro-CMV-GPx4 (C107S)-3×FLAG-WPRE (titer: 4.94E + 08 TU/mL), pSlenti-EFI-EGFP-P2A-Puro-CMV-GPx4 (C28S/C66S/C107S)-3×FLAG-WPRE (titer: 6.60E + 08 TU/mL) or pSlenti-EFI-EGFP-P2A-Puro-CMV-GPx4 (U46C)-3×FLAG-WPRE (titer: 2.93E + 08 TU/mL) was mixed with 5 µg/mL of polybrene (OBiO) and incubated with cells for 12 h in a 5% CO$_2$ cell culture incubator at 37 °C. The stable transfected cell lines were established after 2 weeks selection with puromycin (2 µg/mL).

Intracerebral hemorrhage (ICH) mouse models
Mice were deeply anesthetized with isoflurane (mixture of 70% N$_2$O and 30% O$_2$; 3% induction, 1% maintenance) using an isoflurane vaporizer (RWD, Shenzhen, China) and placed in a stereotaxic frame (RWD) for aseptic surgery. A 0.6 mm burr hole was made in the left striatum, and a 26-gauge needle was inserted into the striatum (coordinates: 0.9 mm anterior, 3.15 mm ventral, and 2.1 mm lateral to the bregma). For collagenase injection model, 0.5 µL of collagenase VII-S (0.1 U/µL, C2399, Sigma-Aldrich) were injected at 0.1 µL/min using a microinjection device (RWD). For autologous blood injection model, blood removed from the tail artery was infused in two-time blocks (6 µL followed by a 5-min pause and then 17 µL followed by a 10-min pause). Twenty-three µL whole blood was injected into the left striatum at a rate of 0.5 µL/min. The needle was slowly removed after an additional 10 min delay. Sham-operated mice received the same head skin incision under isoflurane anesthesia and needle insertion and body temperature was maintained near normothermia (37.0 °C) during surgery with a heating blanket (RWD). All efforts were made to minimize the number of animals used and ensure minimal suffering. Body weight, rectal temperature, and survival rate were recorded for each mouse before and after surgery until the endpoint of experiments.

Stereotaxic injection of viruses
Viruses were obtained from OBiO. Mice were anesthetized using an isoflurane vaporizer. Two bur holes were drilled at left striatum: 1 mm anterior and 1.9 mm lateral of the bregma, and 0.6 mm anterior and 2.25 mm lateral of the bregma. To overexpress Irg1 in striatal neurons in WT mice, the total volume of 1.2 µL of pAAV-SYN-EGFP-P2A-Irg1-3×FLAG (titer: 8.96 + 10^{12} vg/mL), or pAAV-SYN-EGFP-P2A-MCS (titer: 7.84 + 10^{12} vg/mL) were injected into a bur hole at two depth (3.05 mm and 3.25 mm) using an automatic microinjection system at a rate of 0.1 µL/min. The needle was slowly removed after an additional 10 min delay. The craniotomy was sealed with Vetbond Tissue Adhesive (1469SB, 3M, USA), and then sterilized with iodophors and 75% ethanol. The infected area and efficiency of virus were confirmed after 3 weeks of injection. To knock out Irg1 in the striatal neurons, we injected pAAV-SYN-EGFP-P2A-CRE (titer: 3.59 + 10^{13} vg/mL) or pAAV-SYN-EGFP-P2A-MCS (titer: 7.84 + 10^{12} vg/mL) into Irg1$^{fl/fl}$ mice with the same procedure stated above. To overexpress GPx4^{WT} and GPx4^{C66S} in striatum, 2.8 µL of pSlenti-EFI-EGFP-P2A-Puro-CMV-GPx4-3×FLAG-WPRE (titer: 7.03E + 08 TU/mL) and pSlenti-EFI-EGFP-P2A-Puro-CMV-GPx4 (C66S)-3×FLAG-WPRE (titer: 6.60E + 08 TU/mL) were injected into the WT mice.

To exclude the influence of endogenic neuronal GPx4 in WT mice, we first knocked down striatal GPx4 by injection of pscAAV-hSyn-EGFP-miR30shRNA (GPx4)-WPRE (titer: 3.73E + 12 vg/mL) into WT mice with the same procedure stated above. After 1 week, we injected the pscAAV-hSyn-GPx4(WT)-3×FLAG-tWPA (titer: 4.16E + 12) or pscAAV-hSyn-GPx4(C66S)-3×FLAG-tWPA (titer: 3.91E + 12 vg/mL) in the same location.

PLX5622 administration
PLX5622 (HY-114153, MedChemExpress) was formulated in AIN-76A rodent chow by Research Diets at a concentration of 1200 mg/kg, while the standard AIN-76A diet was provided as the control. Mice were provided ad libitum access to PLX5622 (1200 mg/kg) or control diet for 14 days to deplete microglia before ICH, and were maintained on the experimental diets or control diets for the duration of the study. The efficiency of PLX5622 was validated with immunostaining and ~96% of microglia in WT mice were depleted as reported [49].

Metabolites quantification by LC-MS (MRM mode) and MALDI-TOF
TCA metabolites were quantitated at LipidALL Technologies, China. Polar metabolites were extracted by homogenizing ipsilateral hemisphere or corresponding tissue in sham group in acetonitrile: water (1:1, v/v), and then derivatized using 3-nitrophenylhdyrazones and analyzed on a Jasper HPLC-coupled to Sciex 4500 MD system as previously described [50]. Metabolites were ionized in the electrospray ionization mode, with the following source parameters: CUR: 25, CAD: 7, GS1: 35, GS2: 35, IS: -4500, TEM: 550. Derivatized metabolites were separated on a Phenomenex Kinetex C18 column (100 × 2.1 mm, 2.6 µm) using 0.1% formic acid (F0507, Sigma-Aldrich) in water as mobile phase A and 0.1% formic acid in acetonitrile (34851, Sigma-Aldrich) as mobile phase B. The gradient started with 15% B which increases linearly to 100% over 12 min, followed by a re-equilibration at 15% B over 3 min before the next injection. Deuterated standards including d3-pyruvate, d4-succinic acid, d4-citric acid, d3-malic

acid and d4-fumaric acid purchased from Cambridge Isotope Laboratories, as well as $^{13}C_3$-lactate from Sigma-Aldrich, were used as an internal standard for quantification. TCA cycle metabolites were quantified via LC-MRM by referencing to the intensities of spiked internal standards. MRM transitions used for quantification of individual metabolites were provided in Supplemental Table 2.

Itaconate and other metabolites were imaged at Guidon Pharmaceutics, China, frozen brain tissue samples were fixed in three drops of distilled water during the cutting stage. Itaconate (129204, Sigma-Aldrich), Succinate (398055, Sigma-Aldrich), and Malate (PHR1273, Sigma-Aldrich) were included as standards. Brain tissues were sectioned at 12 µm thickness using a cryostat (CM1950, Leica, Germany) at −20 °C. Afterwards, the thawed brain sections were placed in groups on electrically conductive slides coated with indium tin oxide (ITO) (75 mm × 25 mm × 1.1 mm, Resistance value = 10 Ω., GL-1010-1.1, Guluo, China), and the slides with brain sections were dried in a vacuum desiccator for 30 min. MALDI-MSI experiments were performed on a rapifleX MALDI-TOF/TOF MS (Bruker Daltonics, Billerica, MA) equipped with a 10 kHz smart beam 3D laser. Laser power was set to 80% and then fixed throughout the whole experiment. The mass spectra were acquired in negative reflection mode, an accelerating voltage of 20.00 kV, a lens voltage of 11.35 kV, and a reflector voltage of 20.85 kV. The mass spectra data were acquired over a mass range from m/z 80–200 Da. The imaging spatial resolution was set to 50 µm for the brain tissue, and each spectrum consisted of 100 laser shots. MALDI mass spectra were normalized with the total ion current (TIC), and the signal intensity in each image was shown as the normalized intensity. MS/MS fragmentation performed on the rapifleX MALDI-TOF/TOF MS in the LIFT mode were used for further detailed structural confirmation of the identified metabolites.

The global Metabolomics analysis was conducted by Biotree Technologies, China. Firstly, mouse brain tissue was isolated, sonicated, and incubated for 1 h (−40 °C) in extract solution (methanol: water = 3: 1, with isotopically-labeled internal standard mixture). Then, the mixture was centrifuged at 13,800 g for 15 min at 4 °C and the supernatant was collected for LC-MS/MS analysis. LC-MS/MS analysis was performed using UHPLC system (Thermo Fisher Scientific vanquish, USA) with a UPLC HSS T3 column (2.1 mm) × 100 mm, 1.8 µm), coupled with Orbitrap exploris 120 mass spectrometer (Orbitrap MS, Thermo Fisher Scientific). The mobile phase system was consisting of phase A (water containing 5 mmol/L ammonium acetate and 5 mmol/L ammonium hydroxide) and phase B (acetonitrile), and 2 µL sample was injected at 4 °C. MS/MS spectra acquisition was conducted by Orbitrap Exploris 120 mass spectrometer equipped with an acquisition software (Xcalibur, Thermo Fisher Scientific). After being converted to the mzXML format by ProteoWizard, the original data has been analyzed by an in-house program, and the internal MS2 database (biotreedb) was used for metabolite annotation (the cutoff for annotation was 0.3).

RT-qPCR analysis

Total mRNA was extracted from cells or tissues using TRIzol reagent (15596026, life technologies, USA). The cDNA was synthesized using a reverse transcription kit (R223-01, Vazyme, China), and qPCR experiments (7500, Applied Biosystem) were performed according to the instructions. After the reaction was completed, the sample was stored at 4 °C, and the resulting threshold cycle (CT) value was the number of cycles required when the fluorescence signal reached a set threshold. The relative expression amount of each pair of samples was calculated from ($2^{-\Delta\Delta CT}$). The following primers were used: *GAPDH*: TGTTCCTACCCCCAATGTGT (F); TGTGAGGGAGATGCTCAGTG (R). *Irg1*: CAGGAAGGCCAGTGCTCAGTAATC (F); ACCTCCTCGCACCCCCTTTGTATG (R). *xCT*: GCTCGTAATACGCCCTGGAG (F); GGAAAATCTGGATCCGGGCA (R). *GPx4*: CTGCTCTTCCAGAGGTCCTG (F); GAGGTGTCCACCAGAGAAGC (R).

Western blotting

Total protein from cells or tissues was extracted with RIPA (C1053, Applygen, China). Total protein was quantified by BCA protein assay (23228, Thermo Fisher Scientific). All samples were electrophoresed on 10% SDS-PAGE gels before transferred to a polyvinylidene fluoride membrane (1620177, Millipore, USA). Membranes were blocked in 5% skim milk for 60 min at room temperature, and then incubated with primary antibody overnight at 4 °C. The primary antibodies used in this study were as follows: Irg1 (1:500 for cells, 1:100 for tissue, 17805S, Cell Signaling Technology, CST, USA), xCT (1:1000, ab175186, Abcam, USA), GPx4 (1:1000 for cells, 1:500 for tissue, ab125066, Abcam), Flag (1:1000,

F1804, Sigma-Aldrich). After treated with the secondary antibodies: Anti-rabbit IgG, HRP-linked Antibody (1:1000, 7074S, CST) or anti-mouse IgG HRP-linked Antibody (1:1000, 7076S, CST) for 1 h, the bands were observed with Immobilon Western HRP substrate (WBKLS0500, Millipore). The relative intensity of protein signals was normalized to the corresponding loading control intensity and quantified by densitometric analysis with ImageJ software (NIH, USA).

Neurological function evaluations

We assessed neurologic deficit score post-ICH at indicated time points, as previously reported [8]. Briefly, an investigator blinded to the experimental cohort scored all mice on six neurologic tests, including body symmetry, gait, climbing, circling behavior, front limb symmetry, and compulsory circling. Each test was graded from 0 to 4. The maximum deficit score was 24. The motor function tests were also performed with forelimb placement test, hindlimb placement test and wire hanging test by an experienced investigator who was blinded to the experimental groups up to 72 h post-ICH. The forelimb placement test was used to investigate the animals' responsiveness to vibrissae stimulation; Intact animals placed the contralateral forelimb quickly on the tabletop. Placing was quantified as the percentage of successful responses in 10 trials. For the hind limb placing test, the mouse was placed on the edge of a tabletop and the contralateral hind limb was pulled down. The test was scored as follows: immediate pullback of limb = 0, delayed pullback = 1, inability to pull back = 2. Placing was quantified in 10 successful trials; trials were excluded when the animal attempted to turn around or walk away. Results are shown as a total score for each mouse. For wire hanging test [51], the experimental apparatus was a stainless-steel bar (diameter: 2 mm; length: 50 cm) resting on two vertical supports and elevated 37 cm above a flat surface, as described previously. Mice were placed on the bar midway between the supports and were observed for 30 s in each of four trials. The amount of time spent hanging was recorded and scored according to the following criteria: 0, fell off; 1, hung onto the bar with two forepaws; 2, hung onto the bar with an added attempt to climb onto the bar; 3, hung onto the bar with two forepaws and one or both hind paws; 4, hung onto the bar with all four paws and with tail wrapped around the bar; 5, escaped to one of the supports.

Cell death assessments and lesion volume analysis

For in vivo experiments, Fluoro-Jade C (FJC) and Cresyl violet (CV) staining were used to assess cell death at perihematoma region as reported previously [52, 53]. Briefly, mice were euthanized by deep anesthesia, and coronal brain sections were stained with FJC (AG325, Millipore) or CV (C5042, Sigma-Aldrich). Treated brain sections were observed and photographed under a fluorescence microscope (ECLIPSE CI, NIKON, Japan) at an excitation wavelength of 450–490 nm. FJC$^+$ cells or CV$^+$ cells was quantified by average the number of perihematomal positive cells in 24 fields from three coronal sections per mouse [54]. For FJC and CV staining, we acquired at least 9 locations in the perihematomal region per mouse [3 fields (upper, left, and right) per section × 3 sections (bregma 1.70 mm, 0.74 mm, and −0.46 mm) per mouse] for quantifications. The mean value of the 9 fields was calculated and used for statistics. Positively stained cells were counted manually and blindly.

To assess cell death in vitro, MTT, propidium iodide (PI) staining and Live/Dead assays were used. For MTT assay, 2×10^4 cell suspension was added to the 96-well plate. After being treated according to the experimental design, the medium was removed, and a medium containing 20 µL of sterile MTT dye (5 mg/mL, 0793, Amresco, USA) was added. After incubation at 37 °C for 4 h, the MTT solution was removed and 100 µL of DMSO was added to dissolve the formaldehyde crystals. The absorbance at 570 nm was measured with a spectrophotometer (SpectraMax iD5, Molecular DEVICES, USA). For PI staining and Live/Dead Assay, 2×10^4 cell suspension was added to the 96-well plate. After the maturation, the cells were treated according to the experimental design, and 100 ng/mL PI dye (P4170, Sigma-Aldrich) or 2× Live/Dead working solution was added. After incubation at 37 °C for 0.5 h or 15 min, the staining was observed under a microscope (ECLIPSE Ti-U, NIKON, Japan).

Lesion volume analysis

To measure lesion volume, mice were euthanized by deep anesthesia, and coronal brain sections were stained with CV (for neurons) and Luxol fast blue (for myelin, S3382, Sigma-Aldrich) at 16 rostral-caudal levels that were spaced 96 µm apart as reported previously [8]. Sections were digitized with

a 1×objective and analyzed with ImageJ software. The injury volume in cubic millimeters was computed by summation of the damaged areas multiplied by the interslice distance (96 μm).

Lipid ROS and MDA measurement

Treated cells were incubated with diluted BODIPY 581/591 C11 reagent (D3861, Invitrogen) for 0.5 h in a 37 °C cell incubator. After washing 3 times with PBS to sufficiently remove the excess probe, images were taken under a fluorescence microscope (ECLIPSE Ti-U, NIKON, Japan) and the ratio of green fluorescence intensity to red fluorescence intensity was calculated with ImageJ software.

To measure Malondialdehyde (MDA) content, 10 mg tissue or 1×10^6 cells were homogenized on ice in 300 μL of MDA Lysis Buffer (with 3 μL BHT, K739-100, Biovision, USA) and then centrifuged (13,000 g, 10 min). Then, 600 μL of hiobarbituricacid reagent was added into each vial containing standards and sample. After Incubated at 95 °C for 60 min and placed in an ice bath for 10 min, 200 μL reaction mixture were measured at 532 nm using a spectrophotometer. The immunofluorescence was also performed to measure neuronal MDA. Briefly, the frozen coronal slices (16 μm thick) which were sectioned in cryostat were incubated in 56 °C for 1 h. The sections were put into antigen repair solution [0.01 M citric acid buffer (10007118, AR, China), pH 6.0] in water bath at 100 °C. After permeabilized with 1% Triton X-100 (T9284, Sigma-Aldrich) for 15 min, brain sections were blocked in 5% goat serum (C0265, Beyotime, China) for 30 min at room temperature. At last, brain sections were incubated with anti-rabbit NeuN (1:500, 36662, CST), anti-MDA [11E3] (1:200, ab243066, Abcam) primary antibody at 4 °C overnight, and then incubated with goat anti-rabbit 647 (A31634, Invitrogen), goat anti-mouse 594 (A11005, Invitrogen). Images were analyzed with confocal microscope (TCS SP8, Leica) and mean fluorescence intensity (MFI) were analyzed with ImageJ software.

Irg1 distribution measurement

To measure the *Irg1* mRNA distribution, fluorescence in situ hybridization was conducted (Servicebio Technology Co., Ltd, Wuhan, China). Briefly, the frozen coronal slices (8 μm thick) which were sectioned in cryostat (Cryotome E, Thermo Fisher Scientific) and were digested by Protease K (20 μg/mL). And then incubated with 3% H_2O_2 for 15 min at room temperature. After being incubated with prehybridization solution for 1 h at 37 °C, brain sections were hybridized with *Irg1*-probe (RX046941, Servicebio) in a humidity chamber at 37 °C. Then, the hybridization solution was removed, the slices were washed and blocked with blocking serum at room temperature for 30 min. Finally, the slices were incubated with anti-digoxin monoclonal antibodies for 1 h at 37 °C and then tyramide signal amplification for 5 min. After blocked with blocking serum at room temperature for 30 min, PBS solution containing anti-rabbit NeuN (1:500), anti-GFAP (1:500, G3893, Sigma-Aldrich) or anti-Iba1 (1:500, ab153696, Abcam) was added and incubated at 4 °C overnight, and then incubated with goat anti-rabbit 488 (A11034, Invitrogen) or goat anti-mouse 594. Images were analyzed with microscope (ECLIPSE CI, NIKON) and Manders' Colocalization Coefficients were analyzed with ImageJ software.

To measure the Irg1 protein distribution, immunofluorescence was conducted. Briefly, the frozen coronal slices (16 μm thick) which were sectioned in a cryostat were incubated at 56 °C for 1 h. The sections were put into antigen repair solution [0.01 M citric acid buffer, pH 6.0] in the water bath at 100 °C. After permeabilized with 1% Triton X-100 (T9284, Sigma-Aldrich) for 15 min, brain sections were blocked in 5% goat serum for 30 min at room temperature. At last, brain sections were incubated with anti-rabbit Irg1 (1:100), anti-CD68 (1:500, ab53444, Abcam) primary antibody at 4 °C for 48 h, and then incubated with goat anti-rabbit 488 or goat anti-rat 594. Images were analyzed with a fluorescence microscope (ECLIPSE CI, NIKON, Japan) and MFI was analyzed with ImageJ software.

GSH content measurement

The total activity of glutathione (GSH) was measured using a GSH assay kit (DIGT-250, Bioassay system, USA). The reagents were added in sequence according to the instructions. Briefly, 2×10^6 cells were collected by centrifugation at 1000 g for 10 min at 4 °C and washed cells in cold PBS. Lysed cells by sonication in 1 mL cold buffer containing 50 mM phosphate (pH 6-7) and 1 mM EDTA. Centrifuge at 10,000 g for 15 min at 4 °C. The 120 μL supernatant was collected and mixed with 120 μL Reagent A in 1.5 mL EP tubes. Vortex to mix well. If turbidity occurs, pellet 5 min at 14,000 rpm in a table centrifuge. Transferred 200 μL sample/Reagent A mixture into wells of the 96-well plate. Add 100 μL Reagent B. Tapped plate lightly to mix and incubated for 25 min at room temperature. Reaction mixture was measured by spectrophotometer with the absorbance at 412 nm.

GPx activity measurement

The homogenized brain supernatants or cells were used to detect glutathione peroxidase (GPx) activity according to the instructions. Briefly, disrupt tissues or cells in the extract buffer by an Ultrasonic Cell Disruptor (UV-04714-51, Cole-parmer, USA), and then centrifuge at 10,000 rpm, 4 °C for 10 min. The supernatant was collected in a new tube and the agents provided in the GPx assay kit (BC1195, Solarbio) were added follow the instructions. The mixture was incubated for 15 min at room temperature. The mixture was added into wells of the 96-well plate and measured the absorbance at 412 nm with a spectrophotometer.

GPx4 activity measurement

As previously reported [28, 55], 50 million of N2A cells were harvested and lysed by lysis buffer (0.5% TritonX-100, 0.5% sodium deoxycholate salt, 150 mM NaCl, 20 mM Tris-HCl pH 7.5, 10 mM EDTA, 30 mM Na-pyrophosphate, and complete protease inhibitor cocktail). The concentration of protein in the lysate was determined using BCA assay kit. The GPx4-specific substrate phosphatidylcholine hydroperoxide (PCOOH) was prepared by enzymatic hydroperoxidation of phosphatidylcholine by soybean lipoxidase: 22 mL of 0.2 M Tris-HCl, pH 8.8, containing 3 mM sodium deoxycholate and 0.3 mM phosphatidylcholine was incubated 30 min at room temperature. The mixture was loaded on a Sep-Pak C18 cartridge (Waters-Millipore) washed with methanol and equilibrated with water. After washing with 10 volumes of water, phosphatidylcholine hydroperoxides were eluted in 2 mL of methanol. Then, on a 96-well plate, 50 μL (2 μg/μL) cell lysate was incubated in the GPx4 activity assay buffer (0.1% Triton X-100, 100 mM Tris-HCl pH 7.4, 10 mM NaN₃, 5 mM EDTA, 0.6 IU/mL Glutathione reductase, 0.5 mM NADPH, and 3 mM GSH unless otherwise noted) at 37 °C for 10 min.

For drug treatment, hemin, 4-OI or vehicle (0.1% DMSO) was added to the 50 μL (2 μg/μL) cell lysate in GPx4 activity assay buffer (0.1% Triton X-100, 0.1 M KH_2PO_4/K_2HPO_4, pH 7.8, 5 mM EDTA, 0.6 U/mL Glutathione reductase, 0.5 mM NADPH, and 3 mM GSH) before incubation. PCOOH was then added to the mixture to initiate GPx4 reaction. Absorbance of NADPH at 340 nm was determined.

RNA-seq

Primary cortical neurons were treated with vehicle (DMSO), 10 μM 4-OI, 50 μM Hemin or Hemin+4-OI for 24 h, and then collected for RNA-seq analysis (Beijing igeneCode Biotech Co. Ltd, Beijing, China). Sequencing libraries were generated using NEBNext® Ultra™ RNA Library Prep Kit for Illumina® (NEB, USA) following the manufacturer's recommendations.

The mRNA was purified from total RNA using poly-T oligo-attached magnetic beads, and fragmented by divalent cations in NEBNext First Strand Synthesis Reaction Buffer (5×). Then, the first strand cDNA was synthesized by random hexamer primer and M-MuLV Reverse Transcriptase (RNase H), and the second strand cDNA synthesis was subsequently performed with DNA Polymerase I and RNase H. Finally, NEBNext Adaptor with hairpin loop structure was ligated with adenylated DNA fragments to prepare for subsequent hybridization, and the library fragments were purified with AMPure XP system (Beckman Coulter, Beverly, USA) to select cDNA fragments of preferentially 150–200 bp in length.

The PCR was conducted with Phusion High-Fidelity DNA polymerase, purified by the AMPure XP system, and assessed with the Agilent Bioanalyzer 2100 system. The clustering of the index-coded samples was performed on a cBot Cluster Generation System using TruSeq SR Cluster Kit v3-cBot-HS (Illumia) according to the manufacturer's instructions. After cluster generation, the library preparations were sequenced on an Illumina Hiseq 2000/2500 platform and 150 bp/100 bp/50 bp paired/single-end reads were generated. The primary sequencing data were produced using Illumina HiSeqT M and have been deposited in the NCBI Gene Expression Omnibus (GEO, https://www.ncbi.nlm.nih.gov/geo/) under accession number GSE189652. After filtering, the "clean reads" were aligned to the reference sequences with Bowtie2 (Version: v2.2.5) and then calculated gene expression level with RSEM (Version: v1.2.12).

Seahorse analysis

Mouse primary neurons were treated as indicated. After 24 h of treatment, neurons were analyzed in a Seahorse analyzer (Seahorse XFe24, Agilent

Technologies, USA) using commercially obtained plates as recommended by the manufacturer to evaluate glycolysis (Extracellular acidification rate, ECAR) and the oxygen consumption rate (Oxygen consumption rate, OCR). Mouse primary neurons (10^5) were cultured in the XFe24 FluxPak (102342-100, Agilent Technologies), after being treated according to the experimental design, the neurons were washed with XF DMEM medium (103575-100, Agilent Technologies) and incubated with the assay medium at 37 °C in a no-CO$_2$ incubator for 60 min before the assay. ECAR was measured with a Seahorse XF Glycolytic Rate Assay Kit (103344-100, Agilent Technologies, US), and 0.5 µM Rotenone plus Antimycin A (Rot/AA) and 50 µM 2-deoxy-D-glucose (2-DG) were sequentially added. OCR was measured with a Seahorse XF Cell Mito Stress Test Kit (103015-100, Agilent Technologies), and 1.5 µM Oligomycin, 2 µM FCCP, and 0.5 µM Rot/AA were sequentially added. The final data was analyzed in Seahorse Wave and normalized to protein content.

Validation of ITalk modified cysteine(s) on GPx4

Pallets of HEK293T cells with overexpressed WT GPx4 proteins and the corresponding mutants were resuspended in 1 mL ice-cold PBS buffer containing 0.1% Triton. The cells were lysed by sonication on ice and the cell lysates were collected by centrifugation (20,000 g, 30 min) at 4 °C to remove the debris. 1 mL cell lysates (2 mg/mL) were incubated with 1 mM ITalk in 37 °C for 2 h. The resulting lysates were precipitated by 4 mL methanol, 1 mL chloroform and 3 mL Milli-Q water. The precipitated proteins were centrifuged at 4000 g for 15 min at 4 °C and washed twice with 500 µL cold methanol, and resuspended in 1 mL PBS containing 0.4% SDS. 1 mL cell lysates (2 mg/mL) were reacted with 1 mM CuSO4, 100 µM TBTA ligand (07-3215, Strem, USA), 1 mM TCEP (C4706, Sigma-Aldrich) and 100 µM azide-PEG-biotin for 1 h at room temperature. The resulting click-labeled lysates were precipitated by 4 mL methanol, 1 mL chloroform and 3 mL Milli-Q water. The precipitated proteins were centrifuged at 4000 g for 10 min at 4 °C, washed twice with 500 µL cold methanol, and then resuspended in 1 mL PBS containing 1.2% SDS (input). Then, 100 µL streptavidin beads (Thermo Fisher Scientific) were washed for three times with 1 mL PBS, and resuspended in 5 mL PBS, which was added to the protein solution. The beads were incubated with the protein solution for 4 h at 29 °C, then washed with 5 mL PBS for three times, and 5 mL distilled water for three times (elution). The resulting beads were resuspended in 500 µL PBS containing 6 M urea, incubated in 10 mM dithiothreitol (DTT) at 37 °C for 30 min, and added with 20 mM iodoacetamide for 30 min at 35 °C in the dark. The beads were then collected by centrifugation and resuspended in 200 µL PBS containing 2 M urea, 1 mM CaCl$_2$ and 10 ng/uL trypsin (V5280, Promega, USA). Trypsin digestion was performed at 37 °C with rotation overnight and the beads were washed with 200 µL distilled water for three times. Release of the modified peptides from the beads was carried out by incubating the beads with 200 µL of 2% formic acid/water for 1 h with gentle rotation in 25 °C. After centrifugation, the supernatant was collected. Then the cleavage process was repeated, and supernatant was combined. In addition, the beads were washed with 50% acetonitrile/water containing 1% formic acid (400 µL), and the washes were combined with the supernatant to form the cleavage fraction. Sample was dried in a vacuum centrifuge and stored at −30 °C until LC-MS/MS analysis. The "input" and "elution" samples were resolved on 10% SDS-PAGE gels and analyzed by Western blotting with anti-Flag antibodies.

To investigate itaconated sites on GPx4 using LC-MS/MS, purified GPx4^{U46C} mutant protein [56] (500 ng) were incubated with 1 mM ITalk or 4-OI for 4 h. The excessive ITalk or 4-OI was removed by a 10-kDa filter. The protein was incubated with 10 mM DTT at 37 °C for 30 min, alkylated with 20 mM iodoacetamide for 30 min at 37 °C in the dark and then added with 30 µL gel loading buffer before analysis by 10% SDS-PAGE. After staining with Coomassie blue, the gels were cut into slices, and added with 100 µL acetonitrile to completely dry the gel slices for 3 times. Residual acetonitrile was removed by centrifugation in vacuum for 30 min until slices are completely dry. Resuspend 4 µg trypsin in 50 mM ammonium bicarbonate (ABC) solution as final concentration of 10 ng/µL. Add 100 µL trypsin solution to the gel slices at 4 °C for 30 min, then place the sample in 37 °C for 12 h. Transfer the supernatant into a clean tube and add 1% formic acid (50% acetonitrile and 50% ABC solution) to cover the gel slices. Agitate at 1200 rpm at room temperature for 15 min to extract the digested peptides. Repeat the extraction until the gel slices become completely dry (3 times). The extracted peptides were dried in a vacuum centrifuge and stored at −30 °C until LC-MS/MS analysis.

Quantification of selenocysteine on GPx4 was performed by low-pH IAdB labeling and subsequent reductive dimethyl labeling. Briefly,

HEK293T cells with overexpressed WT GPx4 proteins were lysed in 1 mL ice-cold PBS buffer containing 0.1% Triton. Then, 1 mL cell lysates (2 mg/mL) were incubated with 0 or 1 mM itaconate at 37 °C for 1 h. The samples were transferred to a 10 kD ultrafiltration unit (Sartorius, product no. 1708008VS) to remove itaconate by washing with 8 M urea, 100 mM tris(hydroxymethyl)aminomethane (Tris) (pH 8.5), 1 mM EDTA, pH 8.5, four times. After that, proteomes were reduced with 20 mM DTT at 37 °C for 30 min and diluted with an approximately half volume of a buffer containing 200 mM citric acid and 8 M urea (pH 2.0) to a final pH of ~4.0. Afterward, proteins were labeled with 0.1 mM iodoacetamide-desthiobiotin (IAdB) probe at 25 °C with gentle shaking for 60 min in the dark. Free IAdB probe were removed by washing with 8 M urea using a 10 kD ultrafiltration unit as mentioned above. The samples were then alkylated with 5 mM IAA at 35 °C for 30 min. The resulting samples were dissolved in 100 mM Tris (pH 8.5) and digested with trypsin at a 1:100 (w/w) ratio and 1 mM CaCl$_2$ overnight at 37 °C. Subsequently, the peptides were collected in the bottom of ultrafiltration tubes by centrifugation (14,000 g, 20 min) and transferred into 5 mL of PBSN (PBS + 1% NP-40) containing 100 µL of streptavidin agarose beads. After incubation for 4 h at 29 °C, the beads were collected and washed with 3 × 5 mL PBSN, 3 × 5 mL PBS, 3 × 5 mL 100 mM triethylammoniumbicarbonate (TEAB) buffer (Sigma-Aldrich), and suspended in 100 µL of 100 mM TEAB buffer. Then 8 µL of 4% HCHO (Sigma-Aldrich) or D^{13}CDO (Sigma-Aldrich) was added to the vehicle and itaconate-treated samples to be light and heavy labeled, respectively. Then 8 µL of 0.6 M NaBH$_3$CN was added to the samples and samples were incubated at 29 °C for 2 h. After washing with 3 × 5 mL 10% acetonitrile (ACN), the beads were treated with 2 × 100 µL of 50% ACN and 2% formic acid (FA) in water for eluting peptides. The samples were placed on a rotator for 10 min and centrifuged (1400 g, 3 min) to collect the supernatant. The supernatant was dried by centrifugation under a vacuum and then resuspended in 0.1% FA for the subsequent LC–MS/MS analysis. Samples were analyzed by LC-MS/MS on Q Exactive series Orbitrap mass spectrometers (Thermo Fisher Scientific) coupled with EasyNano-LC. Under the positive-ion mode, full-scan mass spectra were acquired over the m/z range from 350 to 1800 using the Orbitrap mass analyzer with mass resolution of 70000. MS/MS fragmentation is performed in a data-dependent mode, of which the TOP 20 most intense ions are selected for MS/MS analysis with a resolution of 17500 using collision mode of HCD. Other important parameters: isolation window, 2.0 m/z units; default charge, 2+; normalized collision energy, 28%; maximum IT, 50 ms; and dynamic exclusion, 20.0 s. For the identification of modification sites in cell lysates, LC-MS/MS data was analyzed by ProLuCID [57] with static modification of cysteine (+57.0215 Da) as well as variable modifications of +324.20491 Da on cysteine. For the identification of selenocysteines on GPx4, IAdB modification (+239.163380) on selenocysteine was set as variable modification. For the identification of modification sites on the purified GPx4 protein, LC-MS/MS data was analyzed by pFind [58] with static modification of cysteine (+57.0215 Da) as well as variable modifications of +238.12051 Da (ITalk) or +242.15181 Da (4-OI) on cysteine. The MS/MS spectra of the peptides containing ITalk/4-OI modification was generated by the pFind software.

Covalent docking of itaconate to mouse GPx4

We used Glide, a module of Schrodinger Suite for covalent docking of itaconate to mouse GPx4 (mGPx4). First, the receptor model of mouse GPx4 was download from RCSB Protein Database Bank (PDB ID 5L71), and the ligand was download from PubChem database. Next, the receptor model was prepared by "Protein Preparation Workflow" module to remove waters and other impurities and to repair the structure reasonably. The ligand was structurally prepared using LigPrep and ionized states were generated in a pH range of 7.0 ± 2.0. Finally, Cys66 of mGPx4 was selected as the reaction residue along with the Michael Addition reaction as the reaction type for covalent docking. The final pose was selected based on the maximum absolute value of cdock affinity and docking score.

Quantification and statistical analysis

Data in this paper were presented as mean ± SD and statistical analyses were performed by GraphPad Prism (version 7.0). The normality of all datasets was assessed using the Shapiro-Wilk test, and subsequent selection of parametric or non-parametric tests was based on this assessment. Unpaired two-tailed Student's t-tests, accompanied by Welch's correction, were utilized for comparing two groups exhibiting normal distribution. For comparisons involving more than two groups, ANOVA with correction for multiple comparisons was applied to parametrically distributed datasets,

while the Kruskal-Wallis test with Dunn's correction was employed for non-parametrically distributed datasets. The exact sample size and the statistical methods are annotated in corresponding figure legends. $p < 0.05$ were considered statistically significant.

DATA AVAILABILITY
All the data used in this manuscript are available from the corresponding author upon reasonable request.

REFERENCES

1. Madangarli N, Bonsack F, Dasari R, Sukumari-Ramesh S. Intracerebral hemorrhage: blood components and neurotoxicity. Brain Sci. 2019;9:316.
2. Yao Z, Bai Q, Wang G. Mechanisms of oxidative stress and therapeutic targets following intracerebral hemorrhage. Oxid Med Cell Longev. 2021;2021:8815441.
3. Martin SS, Aday AW, Almarzooq ZI, Anderson CAM, Arora P, Avery CL, et al. 2024 Heart Disease and Stroke Statistics: A Report of US and Global Data From the American Heart Association. Circulation. 2024;149:e347–e913.
4. Zille M, Karuppagounder SS, Chen Y, Gough PJ, Bertin J, Finger J, et al. Neuronal death after hemorrhagic stroke in vitro and in vivo shares features of ferroptosis and necroptosis. Stroke. 2017;48:1033–43.
5. Li Q, Weiland A, Chen X, Lan X, Han X, Durham F, et al. Ultrastructural characteristics of neuronal death and white matter injury in mouse brain tissues after intracerebral hemorrhage: coexistence of ferroptosis, autophagy, and necrosis. Front Neurol. 2018;9:581.
6. Chen CW, Chen TY, Tsai KL, Lin CL, Yokoyama KK, Lee WS, et al. Inhibition of autophagy as a therapeutic strategy of iron-induced brain injury after hemorrhage. Autophagy. 2012;8:1510–20.
7. Li Q, Wan J, Lan X, Han X, Wang Z, Wang J. Neuroprotection of brain-permeable iron chelator VK-28 against intracerebral hemorrhage in mice. J Cereb Blood Flow Metab. 2017;37:3110–23.
8. Li Q, Han X, Lan X, Gao Y, Wan J, Durham F, et al. Inhibition of neuronal ferroptosis protects hemorrhagic brain. JCI Insight. 2017;2:e90777.
9. Karuppagounder SS, Alin L, Chen Y, Brand D, Bourassa MW, Dietrich K, et al. N-acetylcysteine targets 5 lipoxygenase-derived, toxic lipids and can synergize with prostaglandin E2 to inhibit ferroptosis and improve outcomes following hemorrhagic stroke in mice. Ann Neurol. 2018;84:854–72.
10. Alim I, Caulfield JT, Chen Y, Swarup V, Geschwind DH, Ivanova E, et al. Selenium drives a transcriptional adaptive program to block ferroptosis and treat stroke. Cell. 2019;177:1262–79.e1225.
11. Yang WS, SriRamaratnam R, Welsch ME, Shimada K, Skouta R, Viswanathan VS, et al. Regulation of ferroptotic cancer cell death by GPX4. Cell. 2014;156:317–31.
12. Yang WS, Kim KJ, Gaschler MM, Patel M, Shchepinov MS, Stockwell BR. Peroxidation of polyunsaturated fatty acids by lipoxygenases drives ferroptosis. Proc Natl Acad Sci USA. 2016;113:E4966–4975.
13. Gao M, Yi J, Zhu J, Minikes AM, Monian P, Thompson CB, et al. Role of mitochondria in ferroptosis. Mol Cell. 2019;73:354–63.e353.
14. Homma T, Kobayashi S, Sato H, Fujii J. Superoxide produced by mitochondrial complex III plays a pivotal role in the execution of ferroptosis induced by cysteine starvation. Arch Biochem Biophys. 2021;700:108775.
15. Michelucci A, Cordes T, Ghelfi J, Pailot A, Reiling N, Goldmann O, et al. Immune-responsive gene 1 protein links metabolism to immunity by catalyzing itaconic acid production. Proc Natl Acad Sci USA. 2013;110:7820–5.
16. Zhu Z, Umehara T, Tsujita N, Kawai T, Goto M, Cheng B, et al. Itaconate regulates the glycolysis/pentose phosphate pathway transition to maintain boar sperm linear motility by regulating redox homeostasis. Free Radic Biol Med. 2020;159:44–53.
17. Qin W, Qin K, Zhang Y, Jia W, Chen Y, Cheng B, et al. S-glycosylation-based cysteine profiling reveals regulation of glycolysis by itaconate. Nat Chem Biol. 2019;15:983–91.
18. Liao ST, Han C, Xu DQ, Fu XW, Wang JS, Kong LY. 4-Octyl itaconate inhibits aerobic glycolysis by targeting GAPDH to exert anti-inflammatory effects. Nat Commun. 2019;10:5091.
19. Cordes T, Wallace M, Michelucci A, Divakaruni AS, Sapcariu SC, Sousa C, et al. Immunoresponsive gene 1 and itaconate inhibit succinate dehydrogenase to modulate intracellular succinate levels. J Biol Chem. 2016;291:14274–84.
20. Bambouskova M, Gorvel L, Lampropoulou V, Sergushichev A, Loginicheva E, Johnson K, et al. Electrophilic properties of itaconate and derivatives regulate the IkappaBzeta-ATF3 inflammatory axis. Nature. 2018;556:501–4.
21. Mills EL, Ryan DG, Prag HA, Dikovskaya D, Menon D, Zaslona Z, et al. Itaconate is an anti-inflammatory metabolite that activates Nrf2 via alkylation of KEAP1. Nature. 2018;556:113–7.
22. Daniels BP, Kofman SB, Smith JR, Norris GT, Snyder AG, Kolb JP, et al. The nucleotide sensor ZBP1 and kinase RIPK3 induce the enzyme IRG1 to promote an antiviral metabolic state in neurons. Immunity. 2019;50:64–76.e64.
23. Cordes T, Lucas A, Divakaruni AS, Murphy AN, Cabrales P, Metallo CM. Itaconate modulates tricarboxylic acid and redox metabolism to mitigate reperfusion injury. Mol Metab. 2020;32:122–35.
24. Liu H, Feng Y, Xu M, Yang J, Wang Z, Di G. Four-octyl itaconate activates Keap1-Nrf2 signaling to protect neuronal cells from hydrogen peroxide. Cell Commun Signal. 2018;16:81.
25. Vigil TM, Frieler RA, Kilpatrick KL, Wang MM, Mortensen RM. Aconitate decarboxylase 1 suppresses cerebral ischemia-reperfusion injury in mice. Exp Neurol. 2022;347:113902.
26. He R, Liu B, Xiong R, Geng B, Meng H, Lin W, et al. Itaconate inhibits ferroptosis of macrophage via Nrf2 pathways against sepsis-induced acute lung injury. Cell Death Discov. 2022;8:43.
27. Zhao Y, Liu Z, Liu G, Zhang Y, Liu S, Gan D, et al. Neutrophils resist ferroptosis and promote breast cancer metastasis through aconitate decarboxylase 1. Cell Metab. 2023;35:1688–703.e1610.
28. Ingold I, Berndt C, Schmitt S, Doll S, Poschmann G, Buday K, et al. Selenium Utilization by GPX4 Is Required to Prevent Hydroperoxide-Induced Ferroptosis. Cell. 2018;172:409–22.e421.
29. Qin W, Zhang Y, Tang H, Liu D, Chen Y, Liu Y, et al. Chemoproteomic profiling of itaconation by bioorthogonal probes in inflammatory macrophages. J Am Chem Soc. 2020;142:10894–8.
30. Wu R, Liu J, Wang N, Zeng L, Yu C, Chen F, et al. Aconitate decarboxylase 1 is a mediator of polymicrobial sepsis. Sci Transl Med. 2022;14:eabo2028.
31. Sohail A, Iqbal AA, Sahini N, Chen F, Tantawy M, Waqas SFH, et al. Itaconate and derivatives reduce interferon responses and inflammation in influenza A virus infection. PLoS Pathog. 2022;18:e1010219.
32. Lampropoulou V, Sergushichev A, Bambouskova M, Nair S, Vincent EE, Loginicheva E, et al. Itaconate links inhibition of succinate dehydrogenase with macrophage metabolic remodeling and regulation of inflammation. Cell Metab. 2016;24:158–66.
33. Luo Z, Sheng Z, Hu L, Shi L, Tian Y, Zhao X, et al. Targeted macrophage phagocytosis by Irg1/itaconate axis improves the prognosis of intracerebral hemorrhagic stroke and peritonitis. EBioMedicine. 2024;101:104993.
34. Xiong XY, Wang J, Qian ZM, Yang QW. Iron and intracerebral hemorrhage: from mechanism to translation. Transl Stroke Res. 2014;5:429–41.
35. Salvador GA. Iron in neuronal function and dysfunction. Biofactors. 2010;36:103–10.
36. Stankiewicz JM, Brass SD. Role of iron in neurotoxicity: a cause for concern in the elderly? Curr Opin Clin Nutr Metab Care. 2009;12:22–29.
37. Gaasch JA, Lockman PR, Geldenhuys WJ, Allen DD, Van der Schyf CJ. Brain iron toxicity: differential responses of astrocytes, neurons, and endothelial cells. Neurochem Res. 2007;32:1196–208.
38. Selim M, Yeatts S, Goldstein JN, Gomes J, Greenberg S, Morgenstern LB, et al. Safety and tolerability of deferoxamine mesylate in patients with acute intracerebral hemorrhage. Stroke. 2011;42:3067–74.
39. Selim M, Foster LD, Moy CS, Xi G, Hill MD, Morgenstern LB, et al. Deferoxamine mesylate in patients with intracerebral haemorrhage (i-DEF): a multicentre, randomised, placebo-controlled, double-blind phase 2 trial. Lancet Neurol. 2019;18:428–38.
40. Umbrasas D, Cizas P, Arandarcikaite O, Vanagas T, Borutaite V. Effects of itaconic acid on neuronal viability and brain mitochondrial functions. J Bioenerg Biomembr. 2021;53:499–511.
41. Qu C, Dai E, Lai T, Cao G, Liu J, Kang R, et al. Itaconic acid induces ferroptosis by activating ferritinophagy. Biochem Biophys Res Commun. 2021;583:56–62.
42. Zhang Z, Wu Y, Yuan S, Zhang P, Zhang J, Li H, et al. Glutathione peroxidase 4 participates in secondary brain injury through mediating ferroptosis in a rat model of intracerebral hemorrhage. Brain Res. 2018;1701:112–25.
43. Shin D, Kim EH, Lee J, Roh JL. Nrf2 inhibition reverses resistance to GPX4 inhibitor-induced ferroptosis in head and neck cancer. Free Radic Biol Med. 2018;129:454–62.
44. Kerins MJ, Milligan J, Wohlschlegel JA, Ooi A. Fumarate hydratase inactivation in hereditary leiomyomatosis and renal cell cancer is synthetic lethal with ferroptosis induction. Cancer Sci. 2018;109:2757–66.
45. Lapchak PA, Zhang JH, Noble-Haeusslein LJ. RIGOR guidelines: escalating STAIR and STEPS for effective translational research. Transl Stroke Res. 2013;4:279–85.
46. Sagal J, Zhan X, Xu J, Tilghman J, Karuppagounder SS, Chen L, et al. Proneural transcription factor Atoh1 drives highly efficient differentiation of human pluripotent stem cells into dopaminergic neurons. Stem Cells Transl Med. 2014;3:888–98.
47. Du SQ, Wang XR, Zhu W, Ye Y, Yang JW, Ma SM, et al. Acupuncture inhibits TXNIP-associated oxidative stress and inflammation to attenuate cognitive impairment in vascular dementia rats. CNS Neurosci Ther. 2018;24:39–46.

48. Nakajima H, Kubo T, Semi Y, Itakura M, Kuwamura M, Izawa T, et al. A rapid, targeted, neuron-selective, in vivo knockdown following a single intracerebroventricular injection of a novel chemically modified siRNA in the adult rat brain. J Biotechnol. 2012;157:326–33.

49. Witcher KG, Bray CE, Chunchai T, Zhao F, O'Neil SM, Gordillo AJ, et al. Traumatic brain injury causes chronic cortical inflammation and neuronal dysfunction mediated by microglia. J Neurosci. 2021;41:1597–616.

50. Li B, Li L, Li M, Lam SM, Wang G, Wu Y, et al. Microbiota depletion impairs thermogenesis of brown adipose tissue and browning of white adipose tissue. Cell Rep. 2019;26:2720–37.e2725.

51. Pu H, Shi Y, Zhang L, Lu Z, Ye Q, Leak RK, et al. Protease-independent action of tissue plasminogen activator in brain plasticity and neurological recovery after ischemic stroke. Proc Natl Acad Sci USA. 2019;116:9115–24.

52. Wu H, Wu T, Hua W, Dong X, Gao Y, Zhao X, et al. PGE2 receptor agonist misoprostol protects brain against intracerebral hemorrhage in mice. Neurobiol Aging. 2015;36:1439–50.

53. Wu H, Wu T, Han X, Wan J, Jiang C, Chen W, et al. Cerebroprotection by the neuronal PGE2 receptor EP2 after intracerebral hemorrhage in middle-aged mice. J Cereb Blood Flow Metab. 2017;37:39–51.

54. Chang CF, Cho S, Wang J. (-)-Epicatechin protects hemorrhagic brain via synergistic Nrf2 pathways. Ann Clin Transl Neurol. 2014;1:258–71.

55. Liu H, Forouhar F, Seibt T, Saneto R, Wigby K, Friedman J, et al. Characterization of a patient-derived variant of GPX4 for precision therapy. Nat Chem Biol. 2022;18:91–100.

56. Li C, Deng X, Zhang W, Xie X, Conrad M, Liu Y, et al. Novel allosteric activators for ferroptosis regulator glutathione peroxidase 4. J Med Chem. 2019;62:266–75.

57. Xu T, Park SK, Venable JD, Wohlschlegel JA, Diedrich JK, Cociorva D, et al. ProLuCID: an improved SEQUEST-like algorithm with enhanced sensitivity and specificity. J Proteomics. 2015;129:16–24.

58. Chi H, Liu C, Yang H, Zeng WF, Wu L, Zhou WJ, et al. Comprehensive identification of peptides in tandem mass spectra using an efficient open search engine. Nat Biotechnol. 2018;36:1059–61.

ACKNOWLEDGEMENTS

AUTHOR CONTRIBUTIONS

Conceptualization: Wei C., Xiao Z., Zhang Yanling, Luo Z., Wang C., Yang F., and Li Q. In vitro experiments: Wei C., Lan T., Liu M., and Hu L. Established ICH animal models and performed behavior tests: Xiao Z., Wei C., Luo Z., Shen D., Liu J., and Wang X. Identified GPx4 itaconation: Zhang Yanling, Wei C., Liu D., Hu J., and Wang C. Collected data: Wei C., Xiao Z., Luo Z., Shen D., Liu J., Dai Q., Zhang Yurui, Sun Q., Shi L., and Wu W. Analyzed data: Wei C., Xiao Z., Luo Z., Shen D., Zhang C., Wang P., Wang C., Yang F., and Li Q. Writing–original draft: Wei C., Xiao Z., Zhang Yanling, Luo Z., Wang C., Yang F., and Li Q. Writing—review & editing: Wei C., Xiao Z., Zhang Yanling, Luo Z., Wang C., Yang F., and Li Q. All authors have agreed on the final version to be published.

FUNDING

COMPETING INTERESTS

The authors declare no competing interests.

ETHICS

Our studies did not include human participants or human tissue. All procedures on mice were approved by the Experimental Animal Ethics Committee of Capital Medical University, Beijing, China.

ADDITIONAL INFORMATION

Supplementary information The online version contains supplementary material available at https://doi.org/10.1038/s41418-024-01303-8.

Correspondence and requests for materials should be addressed to Chu Wang, Fei Yang or Qian Li.

Reprints and permission information is available at http://www.nature.com/reprints

Publisher's note Springer Nature remains neutral with regard to jurisdictional claims in published maps and institutional affiliations.